

OPTIMIZATIONS OF ANTENNAS USING HEURISTIC ALGORITHMS
SUPPORTED BY THE MULTILEVEL FAST MULTIPOLE ALGORITHM

A THESIS SUBMITTED TO
THE GRADUATE SCHOOL OF NATURAL AND APPLIED SCIENCES
OF
MIDDLE EAST TECHNICAL UNIVERSITY

CAN ÖNOL

IN PARTIAL FULFILLMENT OF THE REQUIREMENTS
FOR
THE DEGREE OF MASTER OF SCIENCE
IN
ELECTRICAL AND ELECTRONICS ENG.

SEPTEMBER 2015

Approval of the thesis:

**OPTIMIZATIONS OF ANTENNAS USING HEURISTIC
ALGORITHMS SUPPORTED BY THE MULTILEVEL FAST
MULTIPOLE ALGORITHM**

submitted by **CAN ÖNOL** in partial fulfillment of the requirements for the degree of **Master of Science in Electrical and Electronics Eng. Department, Middle East Technical University** by,

Prof. Dr. Gülbin Dural Ünver _____
Dean, Graduate School of **Natural and Applied Sciences**

Prof. Dr. Gönül Turhan Sayan _____
Head of Department, **Electrical and Electronics Eng.**

Asst. Prof. Dr. Özgür Ergül _____
Supervisor, **Elec. and Electronics Eng. Dept., METU**

Examining Committee Members:

Prof. Dr. Gülbin Dural Ünver _____
Electrical and Electronics Engineering Dept., METU

Asst. Prof. Dr. Özgür Ergül _____
Electrical and Electronics Engineering Dept., METU

Prof. Dr. Mustafa Kuzuoğlu _____
Electrical and Electronics Engineering Dept., METU

Assoc. Prof. Dr. Lale Alatan _____
Electrical and Electronics Engineering Dept., METU

Assoc. Prof. Dr. Vakur Behçet Ertürk _____
EE Engineering Dept., Bilkent University

Date: 01.09.2015

I hereby declare that all information in this document has been obtained and presented in accordance with academic rules and ethical conduct. I also declare that, as required by these rules and conduct, I have fully cited and referenced all material and results that are not original to this work.

Name, Last Name: CAN ÖNOL

Signature :

ABSTRACT

OPTIMIZATIONS OF ANTENNAS USING HEURISTIC ALGORITHMS SUPPORTED BY THE MULTILEVEL FAST MULTIPOLE ALGORITHM

Önol, Can

M.S., Department of Electrical and Electronics Eng.

Supervisor : Asst. Prof. Dr. Özgür Ergül

September 2015, 76 pages

In this study, an optimization environment based on heuristic algorithms supported by the multilevel fast multipole algorithm (MLFMA) is presented for different antenna problems involving either excitation or geometry optimizations. The heuristic algorithms are implemented in-house by aiming more effective interactions between electromagnetic solvers and optimization algorithms, instead of black-box interactions. Excitation optimizations of various array geometries for desired radiation characteristics are investigated in numerical experiments involving extremely large optimization spaces. Implemented heuristic algorithms are improved via alternative mechanisms and compared to available toolbox of MATLAB. In addition to excitation optimizations, we consider more challenging optimizations involving geometric modifications. In this context, two different types of pixel antennas are studied and optimized. Furthermore, the designs obtained via optimizations are fabricated in low-cost setups based on commercial inkjet printers. Measurements on fabricated samples demonstrate the effectiveness of the optimizations, as well as the efficacy of the low-cost

production mechanism that fully benefits from the advantages of inkjet printing. Finally, approximate forms of MLFMA are examined for dynamic accuracy control during the optimizations. Effects of using these approximate forms and possible strategies for employing them in order to increase the speed of the optimizations are discussed.

Keywords: Multilevel Fast Multipole Algorithm, Genetic Algorithms, Particle Swarm Optimization, Antenna Optimizations, Array Optimizations

ÖZ

ÇOK SEVİYELİ HIZLI ÇOKKUTUP YÖNTEMİYLE DESTEKLENEN KEŞİFSEL METOTLAR İLE ANTEN OPTİMİZASYONLARI

Önel, Can

Yüksek Lisans, Elektrik ve Elektronik Mühendisliği Bölümü

Tez Yöneticisi : Asst. Prof. Dr. Özgür Ergül

Eylül 2015, 76 sayfa

Bu çalışmada, kaynak veya geometri optimizasyonları içeren anten problemlerinin çözümleri için çok seviyeli hızlı çokkutup yöntemi (ÇSHÇY) ile desteklenen keşifsel metotlardan kurulan bir optimizasyon ortamı sunulmuştur. Elektromanyetik çözücüler ve optimizasyon algoritmaları arasındaki etkileşimi daha etkin biçimde sağlayabilmek amacıyla, keşifsel metotlar sıfırdan programlanmıştır. Çeşitli anten dizgelerinin istenilen ışınım örüntülerini sağlayabilmesi için gerekli kaynak değerleri, çok geniş optimizasyon kümelerinin ele alındığı sayısal deneylerle incelenmiştir. Geliştirilen keşifsel metotlar alternatif mekanizmalarla iyileştirilmiş ve MATLAB'ın hazır keşifsel metotları ile karşılaştırılmıştır. Anten dizgelerinin kaynak değeri optimizasyonlarının yanında, daha zor problemler olan antenlerin geometri optimizasyonları da ele alınmıştır. Bu bağlamda iki farklı piksel anten yapısı çalışılmış ve optimize edilmiştir. Ayrıca, optimizasyon sonucu elde edilen antenler, gümüş-bazlı mürekkeple fotoğraf kağıtlarına basılarak ucuz yolla üretilmiştir. Üretilen antenlerin ölçüm sonuçları optimizasyonların

yüksek kalitesini ve ucuz üretim yönteminin olumlu yanlarını göstermiştir. Son olarak, ÇSHÇY'nin yaklaşık formları, optimizasyonlar esnasında dinamik doğruluk kontrolü sağlayabilmek amacıyla incelenmiştir. Optimizasyonların hızının artırılabilmesi için bu yaklaşık formların kullanımları ve farklı stratejiler tartışılmıştır.

Anahtar Kelimeler: Çok Seviyeli Hızlı Çokkutup Yöntemi, Genetik Algoritmalar, Parçacık Sürü Optimizasyonu, Anten Optimizasyonları, Dizge Optimizasyonları

To my beloved family...

ACKNOWLEDGMENTS

I am deeply indebted to my supervisor, Asst. Prof. Dr. Özgür Ergül, whose invaluable guidance, constant support and encouragement helped me complete this study.

I would like to thank Prof. Dr. Gülbin Dural Ünver, Prof. Dr. Mustafa Kuzuoğlu, Assoc. Prof. Dr. Lale Alatan and Assoc. Prof. Dr. Vakur Behçet Ertürk for taking the time to be on my thesis committee.

I also thank Barışcan Karaosmanoğlu, Tolga Çiftçi, Hilal Kübra Dumanlı, Özer Gökçe, İlyas Genel, Bengisu Eliş, Hüseyin Boyacı and all members of CEM-METU for their cooperation in my studies.

I also thank to ASELSAN Electronics Industries Inc. for its all supports to my graduate study.

I would like to give my special thanks to Damla Alptekin for her unwavering support. My thanks go to Tuğser Kutlu, Hazal Gümüšoğlu and Koray Ertan for their efforts to increase the quality of my life during my graduate studies. Last but not the least, I thank my family for their unconditional love and support.

TABLE OF CONTENTS

ABSTRACT	v
ÖZ	vii
ACKNOWLEDGMENTS	x
TABLE OF CONTENTS	xi
LIST OF TABLES	xiv
LIST OF FIGURES	xv
LIST OF ABBREVIATIONS	xx
CHAPTERS	
1 INTRODUCTION	1
2 THE TOOLS USED IN THE OPTIMIZATIONS	5
2.1 Introduction	5
2.2 Multilevel Fast Multipole Algorithm	5
2.3 Genetic Algorithms	7
2.3.1 Chromosome Representation	8
2.3.2 Initialization of the First Population	8
2.3.3 Selection for Mating	9
2.3.3.1 Roulette Wheel Method	10

	2.3.3.2	Tournament Selection	10
	2.3.4	Crossover	10
	2.3.4.1	Single-Point Crossover	11
	2.3.4.2	Double-Point Crossover	11
	2.3.5	Mutation	11
	2.3.6	Elitism	11
	2.4	Particle Swarm Optimization	12
	2.5	Antenna Modeling	13
	2.6	Remarks	14
3		EXCITATION OPTIMIZATIONS OF ANTENNA ARRAYS . .	15
	3.1	Introduction	15
	3.2	Optimization Mechanism	16
	3.3	Optimizations of a 5×5 Planar Array	18
	3.4	Improvements on GA Operations	22
	3.4.1	Success-Based Mutation	22
	3.4.2	One-to-One Crossover Operations	23
	3.4.3	Family Elitism	24
	3.4.4	Performance of the Improved GA on the 5×5 Array	24
	3.5	Monitoring Parameters and Improving the Performance of GAs	29
	3.6	PSO and Improving Its Performance	30
	3.7	Performance Comparison of GAs and PSOs	34
	3.8	Multi-Objective Optimizations	39

	3.8.1	Dual-Band Optimizations	39
	3.8.2	Shaping Radiation Patterns	42
	3.9	Remarks	44
4		GEOMETRY OPTIMIZATIONS OF PIXEL ANTENNAS . . .	45
	4.1	Introduction	45
	4.2	Optimization Mechanism	46
	4.2.1	Lookup-Table Concept	46
	4.3	Fabrication of Inkjet Antennas	47
	4.4	Optimizations of Cage-Dipole Antennas	49
	4.5	Optimizations of Patch-Pixel Antennas	56
	4.6	Remarks	60
5		ACCURACY CONTROL BY USING APPROXIMATE FORMS OF MLFMA	63
	5.1	Introduction	63
	5.2	Approximate Forms of MLFMA	63
	5.3	Optimizations of the Cage-Dipole Antenna via AMLFMA	65
	5.4	Optimization of the Cage-Dipole Antenna on a $4\lambda \times 4\lambda$ Platform via AMLFMA	68
	5.5	Remarks	70
6		CONCLUSION	71
		REFERENCES	73

LIST OF TABLES

TABLES

Table 3.1 Summary of the Examined GA Versions	31
Table 3.2 Summary of the Examined PSO Versions and Their Applications to a 10×10 Array	33
Table 4.1 Simulation Results of Optimized Antennas For $(\theta, \phi) = (0, 0)$.	52
Table 4.2 Simulation Results of Optimized Antennas For $(\theta, \phi) = (90, 0)$	53
Table 5.1 Performance Summary When Fixed Approximation Factors Are Employed During Optimizations	66
Table 5.2 Different Strategies For the Usage of MLFMA and Its Approximate Forms on the Optimizations of the Antenna Depicted in Figure 4.3	67
Table 5.3 Number of Harmonics Used for Different Values of Approximation Factor For a 5-Level MLFMA	69
Table 5.4 Performance Summary of Different Approximation Factors For the Problem Depicted in Figure 5.1	69
Table 5.5 Results With Different Strategies For the Transmission Coefficient Optimization of the Geometry Shown in Figure 5.1	70

LIST OF FIGURES

FIGURES

Figure 2.1	Block diagram of a standard GA optimizer.	8
Figure 2.2	Block diagram of a particle swarm optimizer	12
Figure 3.1	Block diagram of the proposed optimization environment for excitation optimizations.	17
Figure 3.2	A 5×5 array involving a periodic arrangement of $3 \text{ cm} \times 3 \text{ cm}$ patch antennas. Each antenna is excited via current injection from a port located at its bottom.	19
Figure 3.3	Far-zone electric field values, each corresponding to the unit excitation of a single element while others are passive. All mutual couplings are included in the computations. Far-zone electric field values are plotted in linear scale in order to see the effects of mutual couplings in detail.	20
Figure 3.4	Cost functions with respect to the number of generations when a standard GA is used. Note that the directive gain values are given in linear scale.	21
Figure 3.5	Description of success-based mutations used in the improved GA.	23
Figure 3.6	Crossover operator used in the improved GA.	23
Figure 3.7	Family elitism used in the improved GA.	24

Figure 3.8 Cost functions with respect to the number of generations when the improved GA is used. Note that the directive gain values are given in linear scale.	25
Figure 3.9 Convergence behavior of the improved GA for the optimizations of the 5×5 array. The directive gain of the array is maximized at $\theta = 30$ degrees. Note that the directive gain values are given in linear scale.	26
Figure 3.10 Comparison of the improved genetic algorithm and random trials of constant amplitude excitations for the optimization of the directive gain of the 5×5 array at $\theta = 30$ degrees. Note that the directive gain values are given in linear scale.	26
Figure 3.11 Final optimization results for the 5×5 array. Note that the directive gain values are given in linear scale.	27
Figure 3.12 Optimized radiation patterns of the 5×5 array, where the normalized electric field intensity in the far-zone is plotted on the $z - x$ plane as a function of the bistatic angle. The directive gain values are also indicated in dBi.	28
Figure 3.13 A 10×10 array involving a periodic arrangement of $3 \text{ cm} \times 3 \text{ cm}$ patch antennas.	30
Figure 3.14 Performance summary of different GA versions (see Table 3.1) for the optimizations of the 10×10 array in Figure 3.13. Note that the directive gain values are given in linear scale.	31
Figure 3.15 Convergence behavior when version 16 of GA is used to optimize the directive gain of the 10×10 array in Figure 3.13 at $(\theta, \phi) = (0, 0)$. A total of 100 different trials are shown, as well as the average performance (red). Note that the directive gain values are given in linear scale.	32

Figure 3.16 Directive gain values obtained via GAs, PSOs, and the phase-taper method. Note that the directive gain values are given in linear scale.	35
Figure 3.17 Performance comparison of GA, MATLAB GA, and PSO implementations. Note that the directive gain values are given in linear scale.	36
Figure 3.18 Optimized directive gain values for the 10×10 array at 2.45 GHz via different methods.	37
Figure 3.19 Optimized radiation patterns obtained with on - off optimizations via the improved GA.	38
Figure 3.20 Optimized radiation patterns obtained with the phase optimization via the improved GA.	38
Figure 3.21 Geometry of a dual-frequency array operating at 2.45 GHz and 5.8 GHz.	40
Figure 3.22 Cost functions with respect to the number of generations when the improved GA implementation is used to maximize the directive gain in various directions at 2.45 GHz. Note that the directive gain values are given in linear scale.	41
Figure 3.23 Cost functions with respect to the number of generations when the improved GA implementation is used to maximize the directive gain in various directions at 5.80 GHz. Note that the directive gain values are given in linear scale.	41
Figure 3.24 Optimized directive gain values for the dual-frequency array in Figure 3.21.	42
Figure 3.25 Radiation patterns obtained by dual-frequency optimizations of the array in Figure 3.21 at 2.45 GHz.	43
Figure 3.26 Radiation patterns obtained by dual-frequency optimizations of the array in Figure 3.21 at 5.80 GHz.	43

Figure 3.27 Normalized far-zone electric field obtained via the GA for maximizing the directive gain simultaneously at $\theta = 0$ and 30 degrees while setting a threshold for the side lobes.	44
Figure 4.1 Numbers of lookup table calls in GA optimizations of the directive gain of a cage-dipole antenna at various directions.	47
Figure 4.2 Cured samples of inkjet prints and the dependency of the resistance to the curing duration and temperature.	48
Figure 4.3 Geometry of the cage-dipole antenna and gap locations. An optimized configuration is shown, where green and red colors represent short circuit (no gap) and open circuit (gap), respectively.	50
Figure 4.4 Simulated current distributions and directive gain plots of optimized cage-dipole antennas.	51
Figure 4.5 Two optimized antenna configurations. Induced currents on the antennas as well as radiation patterns on the $z - x$ plane are depicted.	53
Figure 4.6 Optimization of the antenna structure depicted in Figure 4.3 to maximize the cost function in Equation (4.1) for $(\theta, \phi) = (0, 0)$. Both the cost function value and the number of table usages are plotted with respect to generations.	54
Figure 4.7 Power reflection coefficient (dB) for both an optimized configuration and the one without naturally occurring parasitic parts. Note that the simulation results are obtained in free space at 5.8 GHz. . .	54
Figure 4.8 Measured and simulated power reflection coefficient values for the optimized antenna.	55
Figure 4.9 S_{11} and radiation plots obtained via HFSS.	56
Figure 4.10 Geometry of an optimized patch-pixel antenna.	57

Figure 4.11 Cost functions with respect to the number of generations of the optimizations for $(\theta, \phi) = (0, 0)$	58
Figure 4.12 Cost functions with respect to the number of generations of the optimizations for $(\theta, \phi) = (30, 0)$	58
Figure 4.13 Obtained antenna configurations of the optimizations for $(\theta, \phi) = (0, 0)$	59
Figure 4.14 Obtained antenna configurations of the optimizations for $(\theta, \phi) = (30, 0)$	59
Figure 4.15 Far-zone electric field radiated from the optimized antenna simulated with MLFMA. The geometry of the antenna is also shown.	60
Figure 4.16 Measured input impedance of the patch-pixel antenna and the power reflection when it is connected to 50Ω	61
Figure 5.1 A cage-dipole antenna involving a total of 2×40 switches on $21 \text{ cm} \times 21 \text{ cm}$ patch.	68

LIST OF ABBREVIATIONS

MLFMA	Multilevel Fast Multipole Algorithm
AMLFMA	Approximate Multilevel Fast Multipole Algorithm
GA	Genetic Algorithm
PSO	Particle Swarm Optimization
EFIE	Electric Field Integral Equations

CHAPTER 1

INTRODUCTION

Heuristic algorithms are widely used in electromagnetic optimization problems due to their flexibility and ability to cover extremely large optimization spaces. However, they may require thousands of trials for the optimizations to converge satisfactory results. When direct solvers are employed by the heuristic algorithms, the required processing time can be extremely long. In order to obtain fast and accurate optimizations, the full-wave solutions can be performed by accelerated algorithms. As a powerful method, the multilevel fast multipole algorithm (MLFMA) allows for calculations of interactions with a memory and time complexity of $O(N \log N)$. Therefore, a combination of heuristic algorithms and a full-wave MLFMA solver is proposed and examined in this study.

The main purpose of this thesis is to present an optimization environment based on heuristic algorithms supported by MLFMA for different antenna problems involving either excitation or geometry optimizations. The proposed mechanism is applied to the excitation-optimization problems involving three different array geometries, as well as to more challenging geometry optimizations involving two different types of pixel antennas. Effectiveness of the optimizations is demonstrated via numerical experiments. Furthermore, the optimized geometries of the pixel antennas are fabricated via low-cost setups based on inkjet printers and tested in a measurement setup. Finally, a dynamic accuracy control using approximate forms of MLFMA is illustrated for further improvements on the efficiency of the optimizations. The contributions and proposed ideas in this study can be listed as follows.

- Genetic algorithms (GAs) and particle swarm optimization (PSO) methods are implemented in-house to provide flexibility and more effective interactions between electromagnetic solvers and optimization algorithms.
- Alternative techniques for GAs, such as success-based mutation operation, family elitism, and one-by-one crossover, are introduced and utilized to increase the performance of the optimizations.
- A superposition principle is used to reduce the number of full-wave solutions to the number of array elements, while all mutual couplings between the elements are taken into account.
- A lookup table concept, which enables the designer to have a dynamic control ability over the optimization, is introduced.
- In geometry optimizations, the required portions are disconnected by removing the related basis functions, which provides effective optimizations.
- Fabrications of low-cost inkjet antennas by using silver-based toners in commercial printers, as well as the associated challenges, are presented.
- Dynamic accuracy control using approximate forms of MLFMA to increase the efficiency of the optimizations without sacrificing the quality of the results is proposed and investigated.

The organization of the thesis is as follows:

The tools used in the proposed optimization environment including MLFMA, GA and PSO, as well as how we model the antennas are briefly discussed in Chapter 2. In Chapter 3, excitation optimizations of antenna arrays and strategies for increasing the performance of these optimizations by utilizing alternative techniques on the heuristic algorithms are explained. The performance comparison of GA and PSO is also demonstrated on optimization problems involving different array geometries. Chapter 4 presents geometry optimizations of cage-dipole and pixel-patch antennas and introduces the concept of lookup table. The fabrication methods of the optimized antennas via inkjet printing and its challenges are explained. In Chapter 5, a dynamic accuracy control using approxi-

mate forms of MLFMA in order to increase the efficiency of the optimizations is discussed. The thesis is concluded with final notes in Chapter 6.

CHAPTER 2

THE TOOLS USED IN THE OPTIMIZATIONS

2.1 Introduction

In this chapter, we present the tools used in the proposed optimization environment, namely MLFMA, GAs, and PSOs, as well as how we model antennas. First, our MLFMA program, which consists of two parts, namely, setup and solution parts, is briefly explained. Then, the main concepts of GAs and PSOs are discussed with their literature review. Finally, the considerations regarding how we model antennas in this study are explained.

2.2 Multilevel Fast Multipole Algorithm

When an electromagnetic problem involves complex geometries and material types, it can be converted into an equivalent problem using the equivalence theorem. Surface electric and magnetic currents are defined on the boundary of the problem geometry and the original radiation or scattering problem is defined using these equivalent currents. Then, using the Maxwell's equations and the boundary conditions, the surface integral equations can be derived. The unknowns in surface integral equations are the equivalent currents defined via the equivalence theorem.

Surface integral equations are discretized and converted into matrix equations to be solved numerically. The solution of a matrix equation can be obtained by either direct solution methods or iterative methods. Due to the high computa-

tional complexity of direct methods, iterative solutions are preferred. An iterative solution requires a matrix-vector multiplication, which can be performed directly or via an acceleration algorithm. In electromagnetics, a direct computation of a matrix-vector multiplication corresponds to direct calculation of electromagnetic interactions, which has a complexity of $O(N^2)$ for N unknowns. For large problems, $O(N^2)$ complexity is expensive and a low complexity method is required. As a powerful algorithm, MLFMA allows for calculation of interactions with a memory and computation complexity of $O(N\log N)$.

The efficiency of MLFMA is based on the Gegenbauer's addition theorem [1]. The homogeneous-space Green's function is expressed in terms of infinite summation of spherical harmonics, which is called factorization. Then diagonalization, i.e., expansion of spherical harmonics in terms of plane waves, is applied. Based on factorization and diagonalization, calculation of electromagnetic interactions using MLFMA follows three steps; aggregation, translation, and disaggregation. These steps are performed as follows: The radiation patterns of sources (basis functions) are aggregated at radiation centers as outgoing plane waves. These radiated fields are translated into receiving centers and converted into incoming plane waves. Incoming plane waves are disaggregated and received by testing functions. Since the diagonalization brings distance restrictions, interactions in MLFMA are divided into two parts: Near-zone interactions and far-zone interactions. Near-zone interactions are calculated directly and stored in memory. Far-zone interactions are calculated on the fly efficiently using MLFMA, as described above.

In our MLFMA application, the program has two parts, namely, setup and solution parts. The setup part is working as follows:

1. Read the problem geometry model.
2. Construct the multilevel tree structure.
3. Calculate the near-zone interactions.
4. Calculate the translation operators.
5. Construct the right-hand-side vector.

In the solution part, the near-zone interactions are used directly and far-zone interactions are calculated via sequences of aggregation, translation, and disag-

gregation. Each matrix-vector multiplication is performed as follows:

1. Use near-zone interactions for given current coefficients.
2. Aggregate the radiation patterns of the basis functions to the box centers at the lowest level of the tree structure.
3. Aggregate the radiation patterns of the boxes to higher levels using the Lagrange interpolation.
4. Translate the radiated fields between far-field boxes at each level.
5. Disaggregate the translated waves to receiving centers of the boxes using interpolation.
6. Distribute the receiving patterns onto testing points in the lowest level boxes.
7. Perform angular integration to complete the matrix-vector multiplication.

2.3 Genetic Algorithms

GAs are well-known heuristic methods in the literature and used extensively in electromagnetic problems due to their flexibility and ability to explore very large optimization spaces [2]. Block diagram of a simple and standard GA is shown in Figure 2.1.

First of all, a chromosome representation for the optimization parameters should be defined for a GA optimization. Then, a population is initialized randomly and individuals in this initial population are evaluated according to the optimization criteria, where a fitness value is assigned to each individual. The fitness value is used to select parents from the population and a crossover mechanism is applied on successful parents to create new individuals. Following a crossover operation, new individuals are mutated in order to increase the diversity of the population. Crossover and mutation operations continue until a new population is formed. GA continues to create new populations (generations) until an individual with desired characteristics is found or predefined termination criteria are met. Each subpart of GA and their effects on the performance are explained in the following sections.

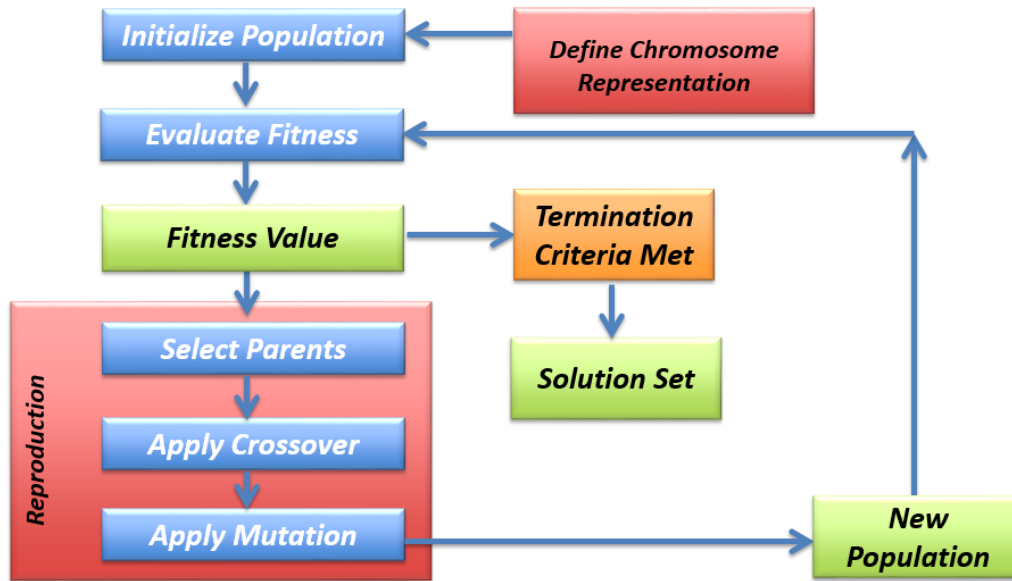


Figure 2.1: Block diagram of a standard GA optimizer.

2.3.1 Chromosome Representation

GAs work on the coded versions of parameters to be optimized rather than directly the parameters themselves. A given parameter domain or space is mapped to chromosomes using a coding technique, where binary coding is the most popular approach [3]. Defining chromosome representation in a meaningful way to the relevant problem is of great importance. Although, it may look like a very simple task, it may profoundly affect the whole performance of the overall algorithm. In general, it is important to define chromosomes as short as possible to reduce the optimization space.

2.3.2 Initialization of the First Population

Since the population size determines the amount of search space that will be explored during one generation, it plays a crucial role in the performance of the GA optimization and it should be arranged accordingly for each problem. Specifically, choosing the population size requires a trade-off between the convergence speed and the diversity of the pool. It is shown that a small population

size may provide fast improvements in the cost function but may lead to an early convergence with a suboptimal solution [4]. This is due to the fact that a small population size contains a small diversity in the gene pool which may cause GA to explore only very limited regions of the optimization space. On the other hand, using large population sizes provides diversity in the pool and often yields stable responses that means GA does not provide significantly different results in each run. However, there are serious issues that should be taken into account when the population size is large. One superior individual, which is far more fit than the rest of the individuals, may change the course of the optimization even in very early generations. The superior individual may force the rest of the population to use its genetic materials, and hence, optimization converges into a region that is solely oriented by the superior individual. As a possible consequence, this region may not contain a good solution and GA may only find a suboptimal solution just like in the small population case but in a longer time [5]. Generally, the optimal population size depends on the solution space and the number of variables to be optimized in a problem [2]. It should be noted that the choice of the population size directly affects the total run time of the optimization when the number of generations is fixed. Therefore, using an optimal population size both improves the performance and reduces the required computational time of GA optimizations.

2.3.3 Selection for Mating

During genetic optimizations, pairs of individuals are selected from the population as parents according to their fitness values. The selection strategy has a significant impact on the overall performance of optimizations. Although the selection strategy should give more chance to better individuals, it should not be based on choosing only the best individuals that would prevent diversity in the population. Thus, a good selection mechanism should also give chance to relatively unsuccessful individuals, without omitting the importance of fit individuals. There are several selection strategies developed and utilized for GAs, such as roulette wheel, linear transformation, tournament selection, and power-law-based selection [6]. Most popular selection strategies in the literature are

roulette wheel selection and tournament selection [2], which are discussed in this study.

2.3.3.1 Roulette Wheel Method

The method may be explained using an analogy with roulette wheels [7]. Its implementation is fairly simple where a random number between 0 and 1 is assigned, which corresponds to the instant when the roulette wheel is spun. Then, an individual is selected at the end of the spin: Each individual has a proportion in the roulette wheel according to its fitness value. Although this method may generally choose the superior individuals, there is still a considerable probability of selection of relatively unfit individuals. Nevertheless, it should be kept in mind that this method is vulnerable for domination especially when there is a significant difference between the fitness value of the best individual and the average fitness value of the population.

2.3.3.2 Tournament Selection

In this method, a subpopulation of n individuals is selected randomly and the individual with the highest fitness value wins the tournament. It is possible to adjust n such that the possibility of the domination effect is minimized [8]. Additionally, it is important to note that the tournament selection has a $O(n)$ complexity while the roulette wheel method has $O(n^2)$. This may be an important factor when GA is used, for problems involving very large number of trials.

2.3.4 Crossover

When a pair of individuals is selected as parents, a pair of children from these parents is created via a crossover operation. Crossover is applied with the probability of $P_{crossover}$ which is generally taken as 0.7-0.9 [2]. There are two types of popular crossover mechanisms, i.e., single-point and double-point crossovers.

2.3.4.1 Single-Point Crossover

The simplest and the most popular crossover technique is single-point crossover. In this technique, a random location in the chromosome of a parent is selected and the portion of the chromosome up to the selected location is copied to the first child, while the rest of the portion is taken from the other parent, and vice versa for the second child.

2.3.4.2 Double-Point Crossover

This technique has the same reasoning with single-point crossover, however instead of a single point, two points are chosen to determine break points for chromosomes. This provides a more controlled distribution of the characteristics from parents to the children than the single-point crossover.

2.3.5 Mutation

After a crossover operation, new individuals are exposed to mutations with a probability of $P_{mutation}$. In a standard mutation operation, each bit in a chromosome is changed with a probability of $P_{mutation}$, which is usually low and in the range from 0.01 to 0.1. Although mutations may increase the diversity in the population, hence they may prevent the domination of one superior individual, strong mutations may also cause the elimination of good genetic materials from the population.

2.3.6 Elitism

The elitism strategy in GAs is first introduced by De Jong [9] and utilized in order to keep the best individual of a population and transfer it to the next population. Since it is possible to lose the best individual during generations due to the random nature of GAs, elitism provides a monotonic increase of the best fitness in the population as a function of generations.

2.4 Particle Swarm Optimization

PSO is a stochastic evolutionary optimization technique based on the movement and intelligence of swarms inspired by the simplified animal social behaviors. PSO was firstly developed by Kennedy and Eberhart in 1995 [10], and then it has been used in various areas [11], including electromagnetics, due to its relatively simple implementation and the obtained fast convergence rates to acceptable solutions.

PSO algorithm is often explained using an analogy with the behavior of birds searching a food source. At the beginning, a group or “swarm” of birds starts to search food source in random directions [12]. Each individual in the swarm remembers the path it traveled as well as the food in these locations. Moreover, the birds communicate with each other regarding the food sources they found during their travels. Therefore, each bird knows the best location that is found by itself and is aware of the best position found by the swarm. Hence the birds go into the regions where the food stocks are high according to both their personal best location and the global best position.

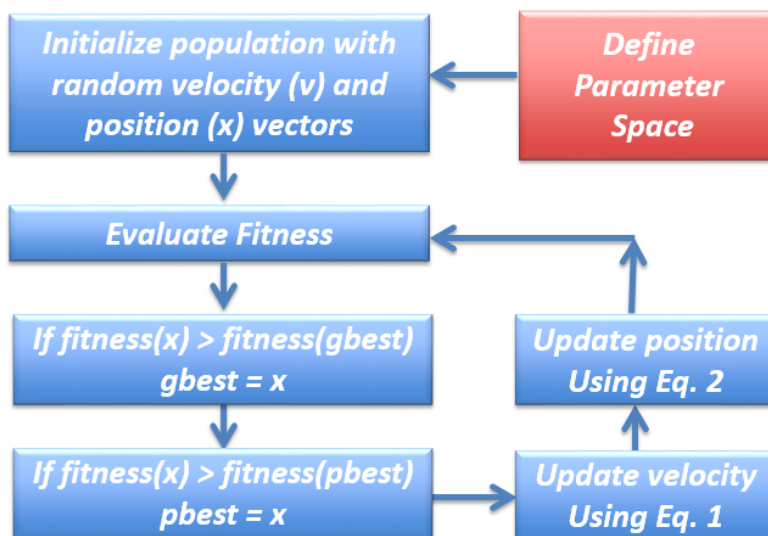


Figure 2.2: Block diagram of a particle swarm optimizer

A simplified block diagram of a PSO is illustrated in Figure 2.2 . Initially, the parameter space is defined according to the optimization problem. Then, a swarm or population is initialized with random velocity and position vectors. According to the optimization goal, each particle in the population is evaluated via the fitness function. If the fitness value of a particle is better than the fitness value of the globally best position found by the swarm or personally best position found by the particle itself considering previous iterations, corresponding values are simply replaced with the current position of the particle. Then, the velocity and position vectors are updated as

$$v_{i+1} = wv_i + c_1r_1(p_{best} - x_i) + c_2r_2(g_{best} - x_i) \quad (2.1)$$

and

$$x_{i+1} = x_i + v_{i+1}t, \quad (2.2)$$

respectively. In these equations, v_i and x_i represent velocity and position vectors of the particles at the i^{th} iteration, w is the inertia weight parameter indicating the effect of a previous velocity vector on the new vector, c_1 is the trust parameter for the individual memory, and c_2 is the trust parameter for the global memory. These parameters have a major influence on the behavior of the optimizer as they determine whether the particles will trust the memory of the swarm or their own memory more [13]. In (2.1) and (2.2), p_{best} and g_{best} store the best positions found by personally and globally in the first i iterations respectively. In addition, r_1 and r_2 are random numbers between 0 and 1, introducing the randomness in PSO. It should be noted that PSO is easier to implement as it does not contain any operator, such as mutation, crossover or selection. The behavior of swarm is directly determined by the velocity and position vectors as governed by (2.1) and (2.2).

2.5 Antenna Modeling

Each antenna is modeled in three-dimensional space via Siemens-NX, which is a powerful CAD tool. The mesh size (the size of the triangles) used in the modeling should be smaller than $\lambda/10$, where λ is the wavelength. Antenna surfaces

are modeled as perfectly conducting and discretized via small triangles on which the RWG functions are utilized to expand the induced electric current density. It should be noted that antenna feeds are modeled by either delta-gap excitations or current injection, and the corresponding electromagnetic problems are formulated with the electric-field integral equation (EFIE) in frequency domain. The full-wave solutions are done either in free space or using a dielectric host medium with an effective permittivity to include dielectric effects. Near-field interactions, which are between nearby basis and testing functions, are performed only once for a given discretization of the full problem and they can be used for all optimizations of the related antenna geometry using MLFMA. Furthermore, preconditioners, radiation/receiving patterns of basis/testing functions, translation operators and right-hand-side vectors are calculated and stored in order to be used during optimizations many times.

2.6 Remarks

In this chapter, tools for electromagnetic optimizations are discussed. Main points regarding this chapter can be listed as follows.

- Both the setup and solution parts of the MLFMA program is explained step by step.
- The concepts of GAs and PSOs are explained with major operations and formulas.
- Full-wave antenna modeling for optimizations is briefly described.

In the next chapter, we consider excitation optimizations of antenna arrays and demonstrate different techniques to improve the performances of GAs and PSOs for efficient optimizations.

CHAPTER 3

EXCITATION OPTIMIZATIONS OF ANTENNA ARRAYS

3.1 Introduction

Antenna arrays can be optimized for desired radiation characteristics by finding appropriate geometrical placement of the elements (antennas) or the excitation values of them [14]. In this study, arrays with a given geometry and fixed positions are optimized by determining a set of source or excitation values that provide the desired radiation characteristics, such as reduction in side-lobe levels, placing nulls in specific directions, and increasing the directive gain at a specific direction [15], [16]. It is well known that the array-factor approach and analytical techniques, such as Taylor and Chebyshev methods, provide rapid designs of excitations of array elements [14]. Although these approaches may be sufficient and convenient for the excitation optimizations of many types of arrays, their accuracy and reliability may deteriorate significantly when mutual couplings between antennas have significant effects on the overall radiation patterns [17]. On the other hand, the interactions between the elements of an array can be modeled very accurately via full-wave solvers based on error-controllable applications of Maxwell's equations. However, in order to obtain an efficient optimization, the full-wave solver should be very efficient.

In this work, we use MLFMA as the required full-wave solver for the optimizations of the antenna arrays [1]. Antenna arrays of finite extent are formulated with EFIE [18] in phasor domain and solved iteratively via MLFMA that pro-

vides accurate and fast matrix-vector multiplications required for iterative solutions. Since the solutions do not have any assumptions or simplifications such as periodicity, infinity or similarity of the array elements, the proposed optimization mechanism can be applied to any type of arrays such as arrays with arbitrary geometrical positions or having different types of elements.

It should be noted that gradient-based approaches could be employed instead of heuristic algorithms for the optimizations. In fact, gradient-based approaches may provide faster convergences than heuristic methods. However, a major disadvantages of them is the development cost since each different optimization goal can be achieved via complex modifications on the optimization code that may be time consuming [19]. Multi-objective optimization problems, multidimensional problems, or problems with multiple solutions may also be difficult for gradient-based methods since they depend on the error surface of the optimization problem [20]. Moreover, gradient-based approaches generally require good initial values for good performances, otherwise they may easily converge to locally optimal solutions [21]. On the other hand, heuristic algorithms use the fitness function of the optimization goal as a closed box. This makes it quite easy to change the optimization goal or make multi-objective optimizations without requiring a change in the optimization code, except the fitness function. In addition, heuristic problems do not depend on error surfaces hence they may solve non-continuous and multidimensional problems. Finally, heuristic algorithms do not necessarily require good initial values which make them especially useful when there is a little information about the problem space. Therefore, an efficient and effective optimization mechanism involving heuristic algorithms supported by MLFMA is proposed and examined in this work.

3.2 Optimization Mechanism

The proposed optimization mechanism mainly consists of heuristic algorithms and the full-wave MLFMA solver. For a given array with fixed positions, heuristic algorithms suggest trials and these trials are evaluated via full-wave solutions by MLFMA according to the optimization criteria to determine the fitness value.

The mechanism is summarized in Figure 3.1 and explained below step by step on a reference problem, which is an optimization of the directive gain of a 5×5 array (see Figure 3.2) in desired directions at 2.45 GHz.

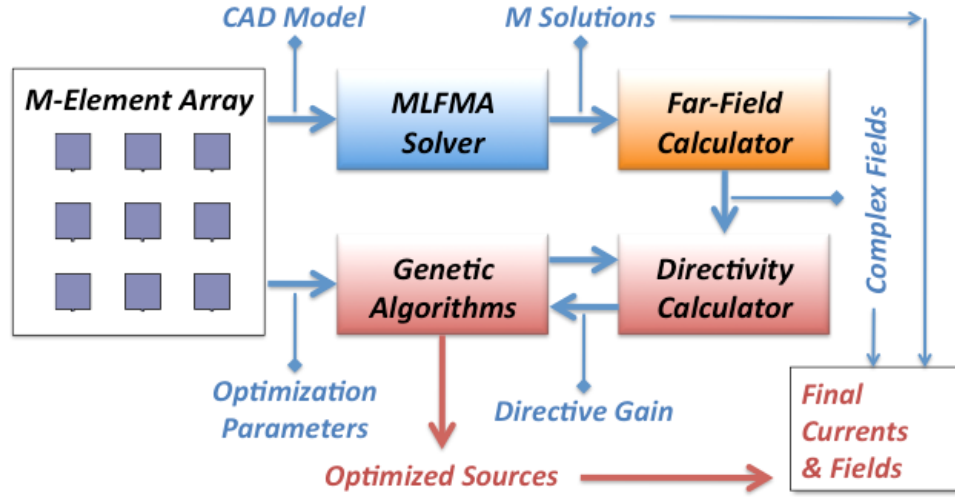


Figure 3.1: Block diagram of the proposed optimization environment for excitation optimizations.

Step 1: The antenna array is modeled in three-dimensional space via Siemens NX, which is a powerful CAD tool. The mesh size (the size of the triangles) used in the modeling should be smaller than $\lambda/10$, where λ is the wavelength.

Step 2: Each trial of a different excitation set corresponds to a different computational problem where excitations of array elements are used to generate the overall radiation pattern. When mutual couplings between array elements are considered in the full-wave solutions, each solution creates a unique current distribution on the antenna surfaces. Moreover, it is possible to reduce the number of current density computations to the number of array elements without neglecting mutual couplings by utilizing superposition principle. For this purpose, each element in the array is excited with a unit source, while all others are passive (they are fed with zero sources). Thus, only a total of M full-wave solutions are required for an array of M -elements per frequency. Once all these solutions are completed, obtained unique current distributions are used

to determine complex far-field radiation patterns. These patterns are stored in the memory to be used many times during optimizations. According to the optimization purpose, these complex far-field radiation patterns may be used directly or to calculate other radiation properties such as directive gains and side-lobe levels. An overall radiation pattern corresponding to any excitation set can be found as a combination of the stored complex far-field patterns.

The radiation problems are formulated by using EFIE, which is suitable for open surfaces with zero thickness. After the triangulation of the surfaces, RWG functions are employed to expand the electric current density. The resulting dense matrix equations are solved iteratively, where MLFMA is used to accelerate matrix-vector multiplications and to reduce the computational complexity to a linearithmic level.

The first two steps may be considered as the setup stage for the optimization mechanism because they are performed only once for a given array structure at a fixed operation frequency.

Step 3: When the setup stage of the optimization mechanism is completed, the aim is to determine the excitation values for each element of the array according to the optimization goal via heuristic algorithms. Specifically for a given array of M elements, there are M complex excitation coefficients and an overall radiation pattern corresponding to any set of excitation coefficients may be found by superposing complex far-fields obtained in Step 2. Each trial suggested by heuristic algorithms which corresponds to an excitation set for the array is evaluated according to the fitness function. In this work, GA and PSO are used as heuristic algorithms due to their rising popularity in electromagnetics society and their superior performances with both binary-coded parameters and continuous parameters, respectively [22].

3.3 Optimizations of a 5×5 Planar Array

The proposed optimization environment is demonstrated by optimizing the directive gain at the desired angles of a 5×5 array of metallic patch monopole

antennas. Throughout this chapter, these antennas are mentioned as patch antennas. It is important to note that these patch antennas do not have any substrate or ground plane. GAs are used for the optimizations.

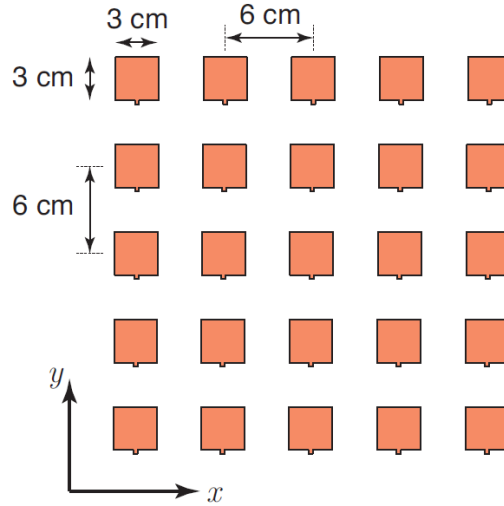


Figure 3.2: A 5×5 array involving a periodic arrangement of $3 \text{ cm} \times 3 \text{ cm}$ patch antennas. Each antenna is excited via current injection from a port located at its bottom.

Figure 3.2 illustrates a 5×5 array of patch antennas that is used as a test problem for the optimization mechanism. The patch antennas of size $3 \text{ cm} \times 3 \text{ cm}$ are arranged periodically with 6 cm periods. The dimensions of each patch correspond to $\lambda_0/4 \times \lambda_0/4$ where λ_0 is the free space wavelength at the operating frequency. The optimization goal for this array is to maximize the directive gain in various desired directions while the operation frequency is 2.45 GHz . First, the geometry of the 5×5 array of patch antennas is modeled via Siemens-NX, in which there are 6350 triangles after the triangulation of the surfaces. 8950 RWG functions are employed to model the entire array. Complex far-fields that are found by feeding each element with a unit current source at 2.45 GHz while all others remain passive are shown in Figure 3.3.

Since the optimization goal is to maximize the directive gain at desired directions, the directive gain is used directly as the fitness function. For the optimiza-

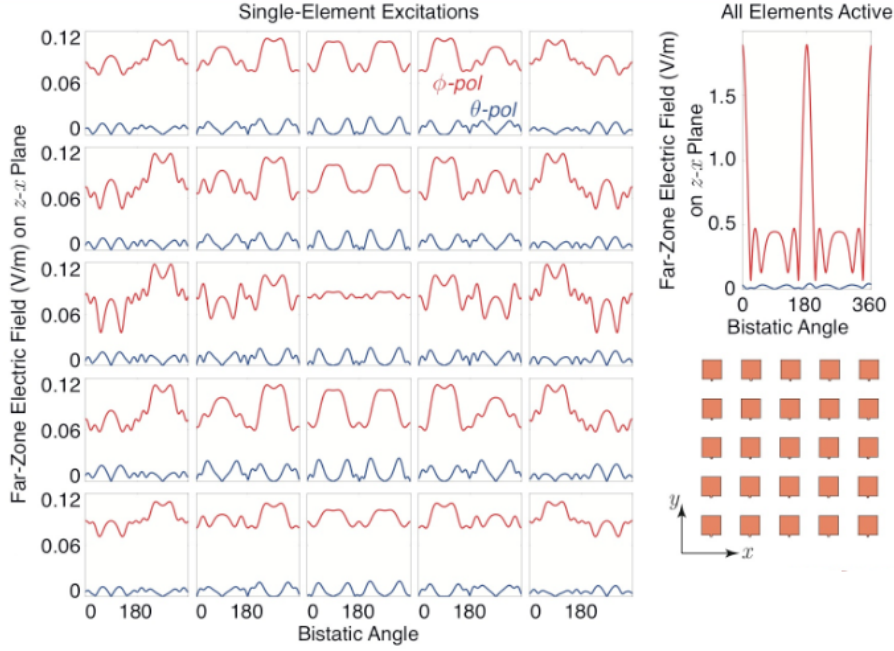


Figure 3.3: Far-zone electric field values, each corresponding to the unit excitation of a single element while others are passive. All mutual couplings are included in the computations. Far-zone electric field values are plotted in linear scale in order to see the effects of mutual couplings in detail.

tions, first we use a standard GA. Excitation sets are coded as chromosomes, where both amplitude and phase parts of the excitation of each element are represented with 7 bits in binary coding. The domain for the phase and amplitude parts are restricted as $[0, 2\pi]$ and $[0, 1]$, respectively. This corresponds to an optimization space with 2^{350} different possibilities. A population size of 80 is chosen after some parametric trials. Moreover, the classical roulette wheel method is used as the selection mechanism and the single-point crossover is utilized along with a standard mutation with 0.05 rate. In addition, the best individual is preserved and transferred to the next population following an elitism strategy. In these trials, 2000 generations are used for each optimization.

Figure 3.4 illustrates the cost functions with respect to the number of generations when the standard GA described above is used for the 5×5 array to maximize its directive gain at desired directions. Although the standard GA provides good fitness values for smaller values of θ such as 0, 5, 10 degrees, it cannot improve the fitness values for wide angles. As an example, the optimization at $\theta = 60$

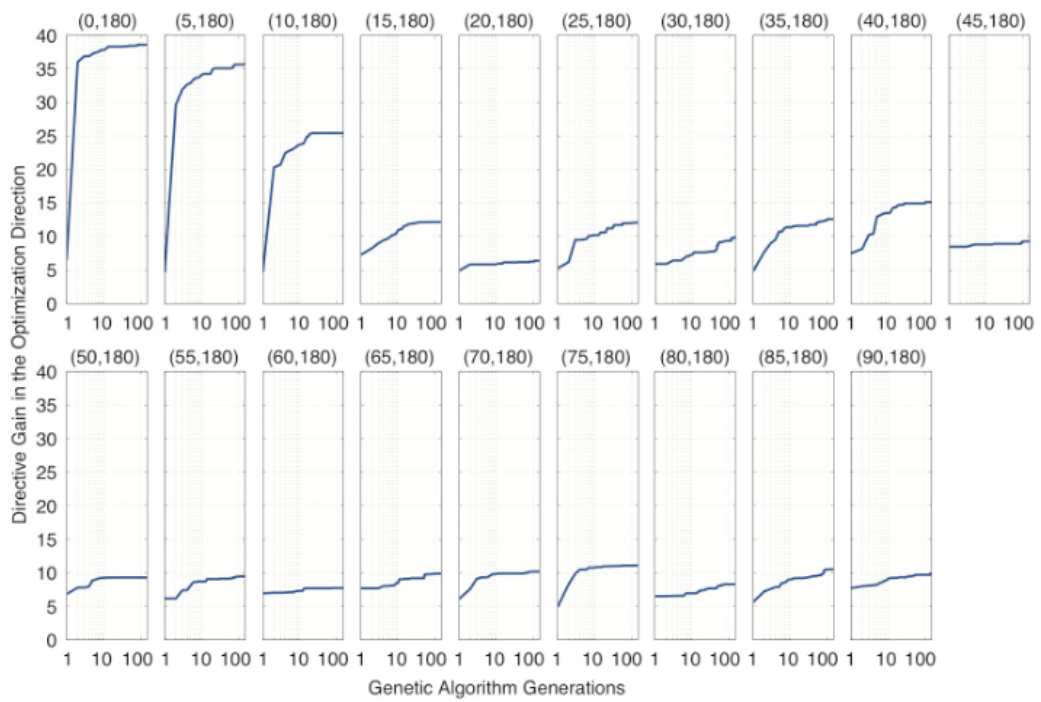


Figure 3.4: Cost functions with respect to the number of generations when a standard GA is used. Note that the directive gain values are given in linear scale.

degrees does little improvement on the best fitness value during 2000 generations. When the populations at each generation of the unsuccessful optimizations are examined, it is observed that the diversity diminishes very quickly. Especially, when a population contains a successful individual and relatively unsuccessful individuals, the successful one dominates the pool during the selection stages. This prevents the formation of new individuals with different characteristics in the populations; hence the optimization spaces are not covered efficiently. Another important observation from these results is that, sudden increases in the fitness values such as the jump for $\theta = 0$, are usually due to the random nature of GAs.

3.4 Improvements on GA Operations

In order to increase the performance of GAs, the optimization space should be covered more efficiently. This can be achieved by maintaining the gene diversity in pools during the generations. For this purpose, different mutation, crossover, and elitism strategies are proposed and tested in this work.

3.4.1 Success-Based Mutation

Instead of a single mutation rate (that is fixed to 5% in the standard GA used in the 5×5 array optimization problems), different mutation rates in the same pool are used to accelerate convergences by maintaining the diversity in pools. Specifically, heavy, moderate, and light mutation rates are applied to individuals, depending on their success rates. Individuals with low success rates are exposed to heavy mutations with 25-30% rates, i.e., each chromosome bit is changed with 25-30% probability, while more successful individuals are mutated less (e.g., 5% rates for the most successful individuals) to maintain the stability. For moderately successful individuals, collective mutations schemes, e.g., changing a portion of the chromosome rather than bit-by-bit mutations, are employed so that badly arranged portions can be directly eliminated. These are simply illustrated in Figure 3.5.

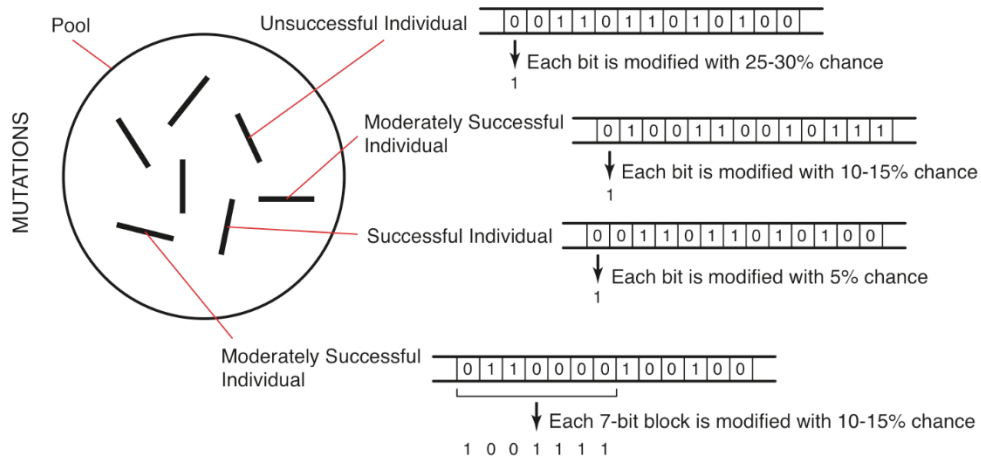


Figure 3.5: Description of success-based mutations used in the improved GA.

3.4.2 One-to-One Crossover Operations

Instead of a popular single-point or double-point crossover schemes, bit-by-bit crossover operations between selected parents to generate children are utilized. Specifically, after a crossover is decided with a rate of $P_{crossover}$ for a given pair of individuals, all corresponding bits are exchanged with 50% probability as illustrated in Figure 3.6. This way, the variety of individuals in the pool increases significantly, leading to more efficient optimizations. Moreover, this crossover mechanism provides a more stable and controlled exchange of characteristics between parents and children.

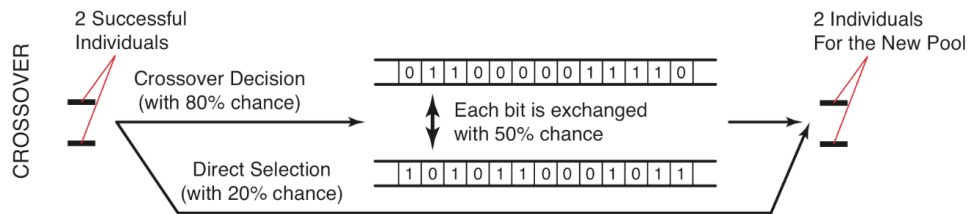


Figure 3.6: Crossover operator used in the improved GA.

3.4.3 Family Elitism

In addition to reserving the most successful individuals for the next generations, proposed strategy, which we call family elitism, forces them to mate. Specifically, for a given pool at a specific generation, this strategy allows two individuals and their children to survive in the next generation as shown in Figure 3.7. This approach guarantees the quality of the pool during the entire optimization process and ensures a better increase in the average success of the population as a function of generations.

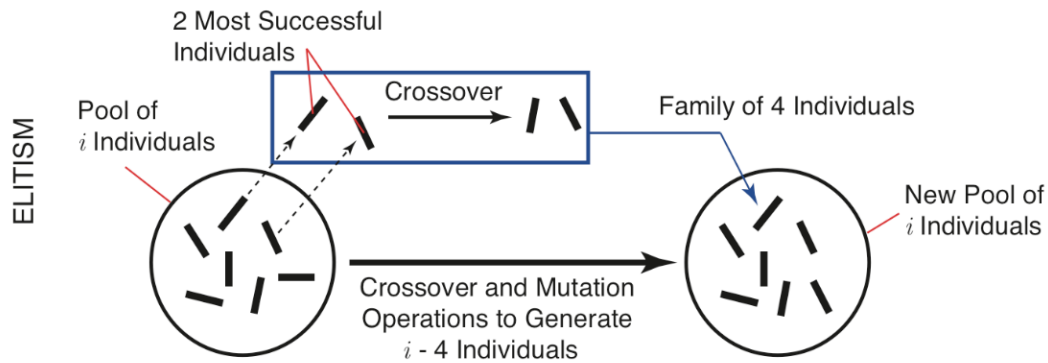


Figure 3.7: Family elitism used in the improved GA.

3.4.4 Performance of the Improved GA on the 5×5 Array

After introducing new mutation, crossover, and elitism strategies, optimizations at each angle are improved as shown in Figure 3.8. In these results, fitness values grow progressively with respect to generations, indicating that more successful individuals are formed almost in each generation. When the populations are examined, it is seen that a domination does not occur thanks to the success-based mutations and one-to-one crossovers. Hence, the diversity of the population does not vanish, allowing the GA to cover the solution space more efficiently.

Another important performance criteria for GAs is the convergence behavior,

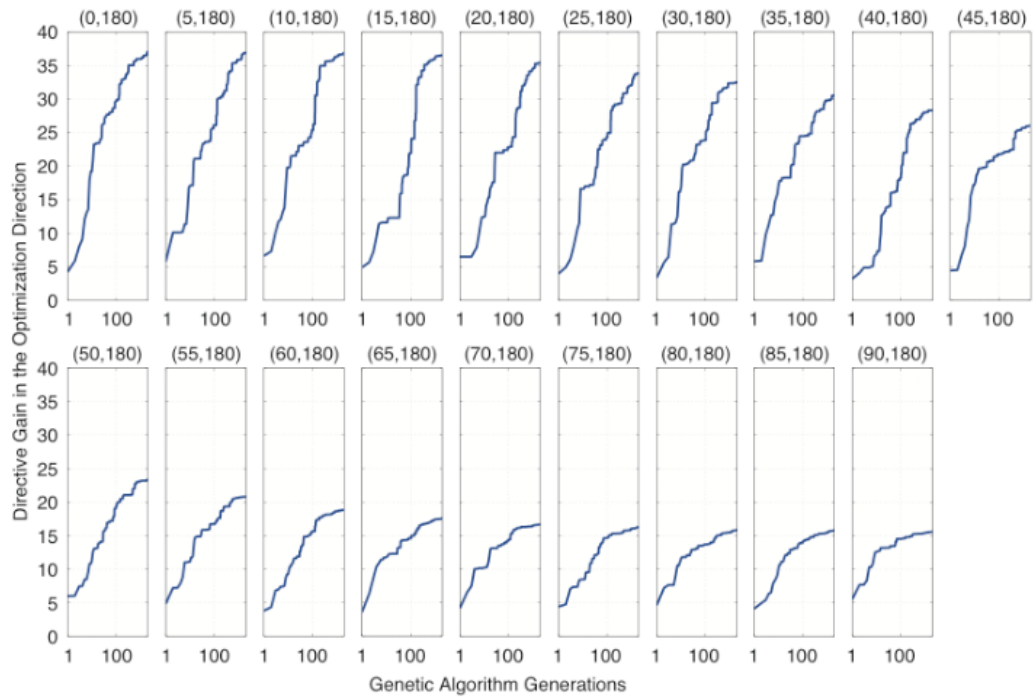


Figure 3.8: Cost functions with respect to the number of generations when the improved GA is used. Note that the directive gain values are given in linear scale.

which shows whether an optimization is stable or not. Due to its random nature, it is possible for a GA to find a good solution even for a very challenging problem. However, the desired performance for a well-designed GA is to find optimal results that are close to each other for different runs. Such a stability test for the improved GA is shown in Figure 3.9. It can be observed that the improved GA converges to a very limited range even for 50 different optimizations, proving the stability of the optimizations.

Since GAs are heuristic methods rather than deterministic, they do not guarantee that the optimized results are the best possible values. Therefore, it is beneficial to compare the optimized results with a large number of random trials. For that purpose, the optimization of the directive gain at $\theta = 30$ degrees is chosen as a reference problem. In Figure 3.10, it is seen that the maximum

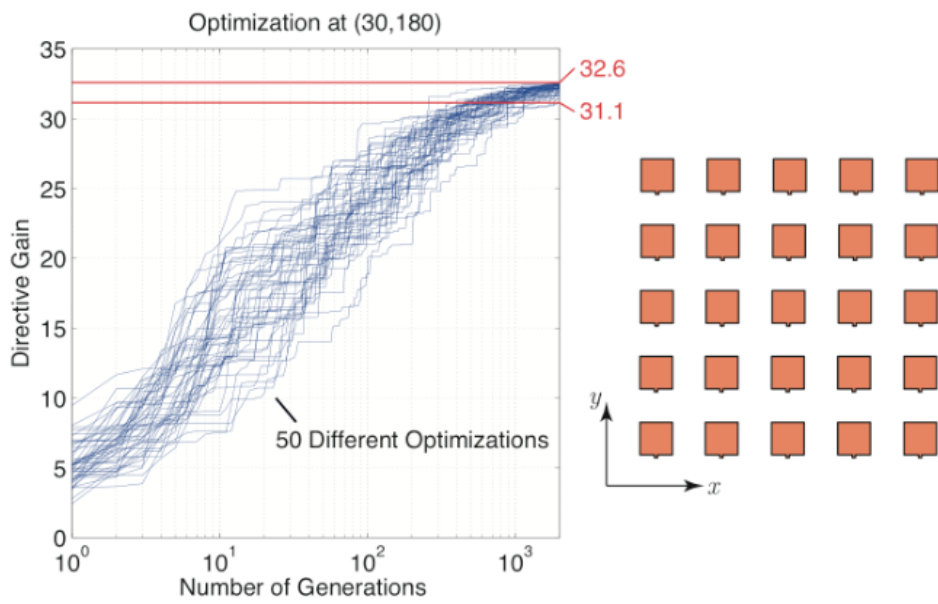


Figure 3.9: Convergence behavior of the improved GA for the optimizations of the 5×5 array. The directive gain of the array is maximized at $\theta = 30$ degrees. Note that the directive gain values are given in linear scale.

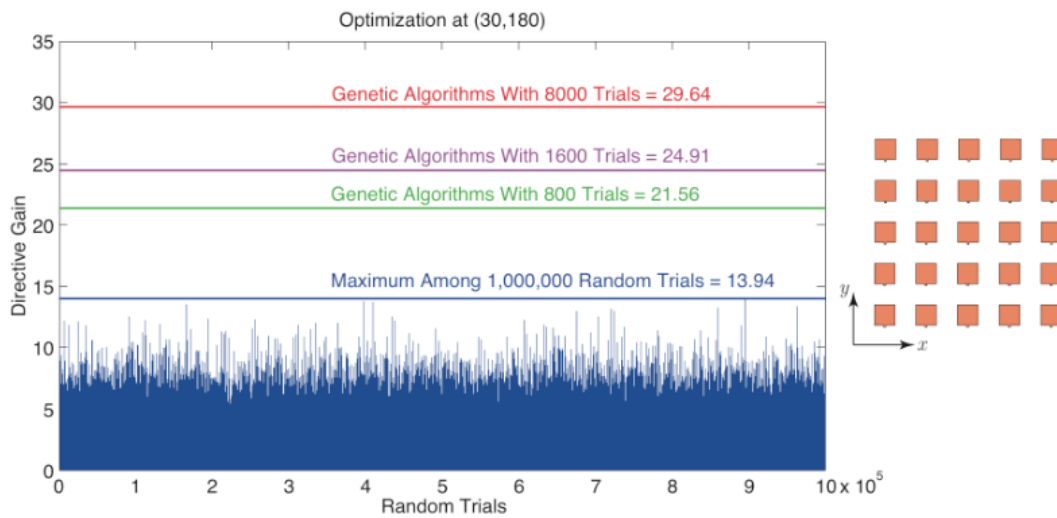


Figure 3.10: Comparison of the improved genetic algorithm and random trials of constant amplitude excitations for the optimization of the directive gain of the 5×5 array at $\theta = 30$ degrees. Note that the directive gain values are given in linear scale.

value among one million random trials is 13.94, while the average is 3.23. On the other hand, the improved GA provides fitness values of 21.56, 24.91, and 29.64 in only 800, 1600, and 8000 trials, respectively. In these results, the average of 10 GA runs are used so that the performance measurement of the improved GA is reliable. Moreover, we emphasize that the standard GA cannot find a better value than 13.94, indicating the necessity of improvements.

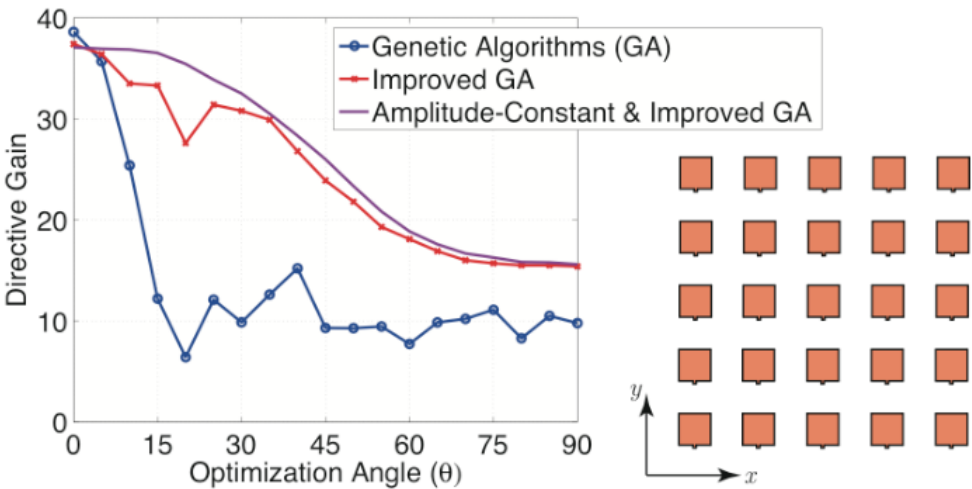


Figure 3.11: Final optimization results for the 5×5 array. Note that the directive gain values are given in linear scale.

In order to observe the effect of the size of the solution space, the improved GA is further tested by optimizing the phases of the excitations when the amplitudes are unity in the 5×5 array. This corresponds to a reduction of the optimization space from 2^{350} to 2^{175} . The results are improved, especially at some difficult angles, such as 20 degrees, as depicted in Figure 3.11. Finally, Figure 3.12 depicts the radiation patterns obtained with the improved GA for constant-amplitude optimizations.

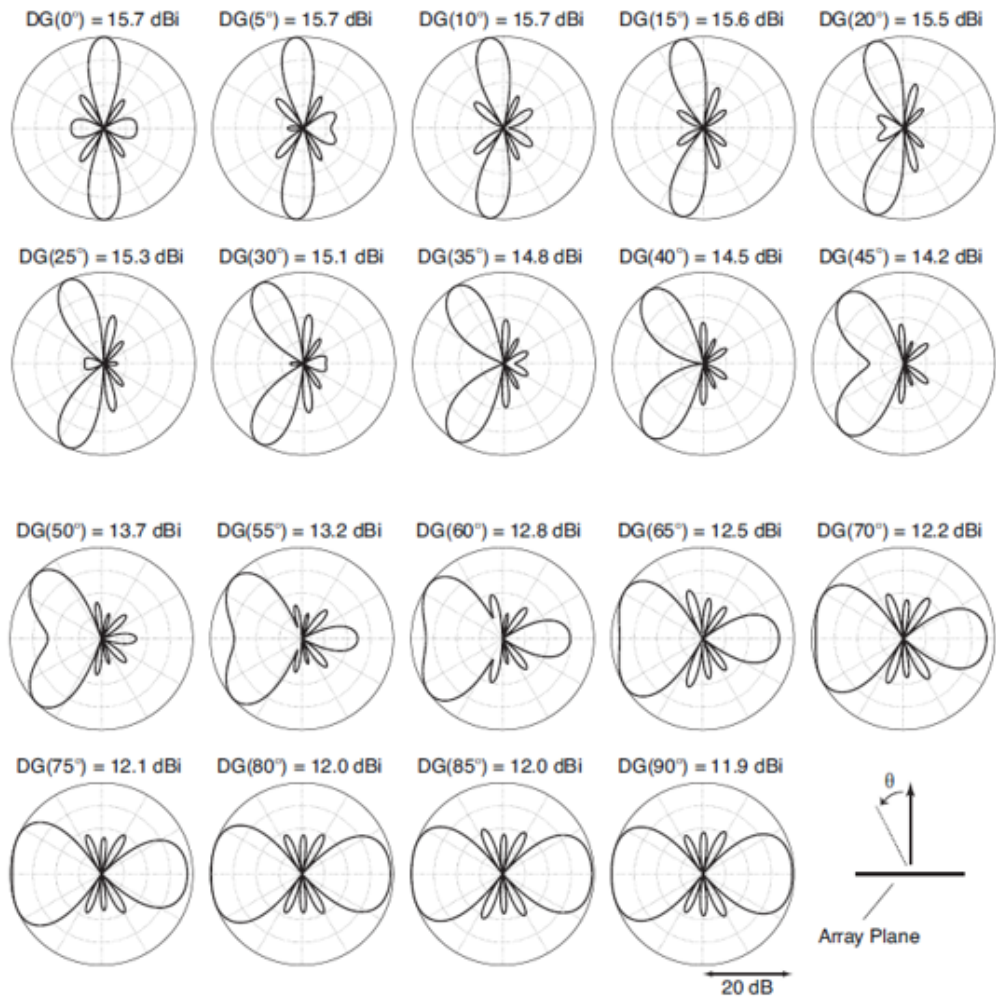


Figure 3.12: Optimized radiation patterns of the 5×5 array, where the normalized electric field intensity in the far-zone is plotted on the $z - x$ plane as a function of the bistatic angle. The directive gain values are also indicated in dBi.

3.5 Monitoring Parameters and Improving the Performance of GAs

Since GA may not perform well for all problems, it is important to know how to monitor its parameters and their effects on the optimizations. One of the major problems encountered when using GAs is early convergence to suboptimal solutions. If a GA optimization gets an early convergence before finding an adequate solution, there may be a need to enlarge the explored regions in the optimization space. In order to do this, pool sizes, mutation rates or reproduction mechanisms can be changed. Moreover, the diversity of a pool directly affects the possible regions to be explored; hence it is desirable to maintain the diversity during generations. As discussed before, the dominance of a superior individual may diminish the diversity rapidly and this should be avoided as much as possible. During the development studies, fitness values of the best individuals and the average fitness values of the populations in each generation, as well as the chromosomes of the individuals in the populations, are stored in tables. Keeping the average fitness values of populations is very beneficial to observe the domination effect. When the average fitness value of a population is relatively low in comparison to the best individual, there is a significant chance of the undesired domination effect. Since the chromosomes in each population are stored, a diversity parameter can be defined in order to observe when the diversity of the pool is reduced. Such a metric can be defined as the total number of bits of all individuals in the population that are different from those of the best individual [23].

In order to test GAs and the developed optimization mechanism for a more challenging problem, where the solution space is extremely large, 10×10 array is considered, where the operation frequency and the size of the patches are same as those in the 5×5 array studies. Specifically, phase optimizations are performed in order to increase the directive gain at $(\theta, \phi) = (0, 0)$, which corresponds to an optimization space with 2^{700} possibilities. Figure 3.13 depicts the geometry of the array.

The total number of trials for each optimization is limited to 80,000 for a fair comparison of the different versions of GAs. Moreover, each optimization is

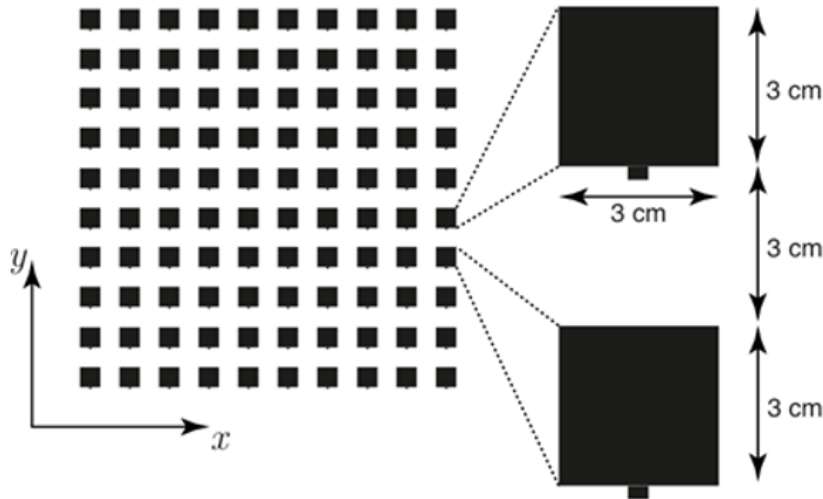


Figure 3.13: A 10×10 array involving a periodic arrangement of $3 \text{ cm} \times 3 \text{ cm}$ patch antennas.

made 10 times and both the average and maximum results obtained by the optimizations are given. The results are listed in Table 3.1 and depicted in Figure 3.14. As shown in these results, GAs can be improved via a step-by-step development process involving the change of crossover operations, mutation strategies, selection schemes, and pool sizes. Table 3.1 shows that final GA version provides directive gain values of 165 (22 dBi) which is the best possible value according to Kraus' formula. We conclude that GA itself needs an optimization of its parameters (as in evolutionary GA) and operations in order to be efficient. Convergence behavior of the final GA version is also shown in Figure 3.15.

3.6 PSO and Improving Its Performance

PSO is another popular approach that we use in our optimizations. As in all heuristic algorithms, performances of PSOs as well as their stability can be improved via proper selections of optimization parameters. Since the behavior of a PSO is determined by the velocity and position vector equations, parameters of these equations can be optimized for better performances. Some of the examined versions of PSOs in this study are listed in Table 3.2 for the optimizations of

Table3.1: Summary of the Examined GA Versions

GA No	$\theta = 0$ Max	$\theta = 0$ Mean	Size	Crossover	Mutation	Selection
1	13.7	9.95	20	2 point	Standard	WhC
2	15.2	10.0	20	1 point	Standard	WhC
3	55.6	33.9	40	one-to-one	Standard	WhC
4	64.9	55.5	80	one-to-one	Standard	WhC
5	99.3	74.2	100	one-to-one	Standard	WhC
6	104	91.9	20	one-to-one	Standard	WhC
7	118	102	200	one-to-one	Standard	WhC
8	147	133	20	one-to-one	Standard	WhC
9	146	135	80	one-to-one	Standard	WhC
10	150	136	80	one-to-one	Standard	WhC
11	147	139	80	one-to-one	Standard	WhC
12	152	142	80	one-to-one	Standard	WhC
13	163	159	80	one-to-one	Standard	TOS 25%
14	163	159	80	one-to-one	Standard	TOS 10%
15	164	160	80	one-to-one	Standard	TOS 20%
16	165	163	80	one-to-one	Standard	TOS 20% and WhC

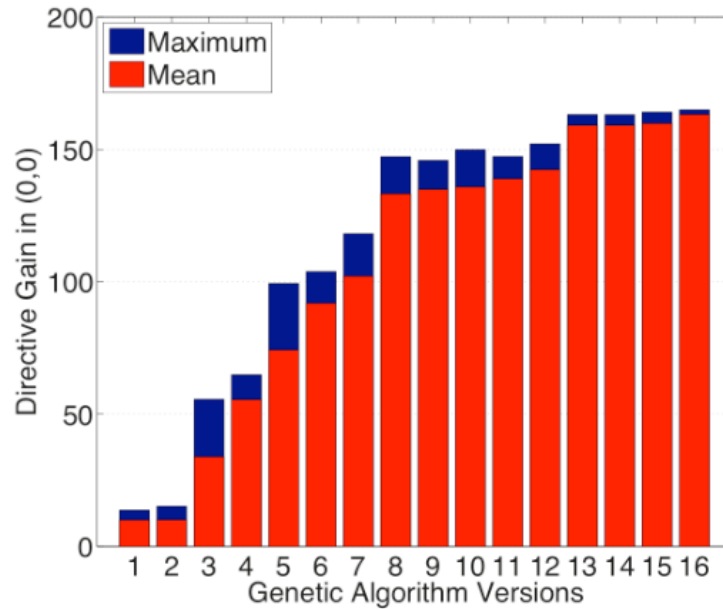


Figure 3.14: Performance summary of different GA versions (see Table 3.1) for the optimizations of the 10×10 array in Figure 3.13. Note that the directive gain values are given in linear scale.

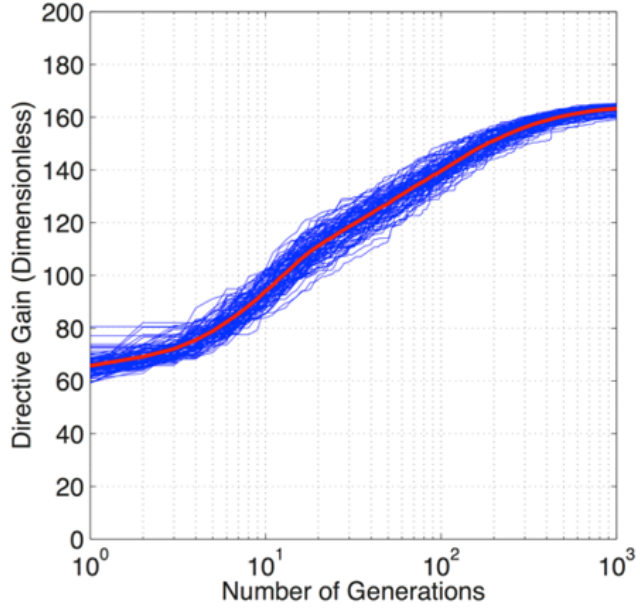


Figure 3.15: Convergence behavior when version 16 of GA is used to optimize the directive gain of the 10×10 array in Figure 3.13 at $(\theta, \phi) = (0, 0)$. A total of 100 different trials are shown, as well as the average performance (red). Note that the directive gain values are given in linear scale.

the 10×10 array in Figure 3.13.

The number of particles in the swarm has a major influence on the performance of PSO because the swarm makes its first movement into a direction based on particles. In order to see this effect, different numbers of particles as 200, 500, 1000, 2000, 2500, and 5000 are selected and the corresponding performances are investigated in versions 1-6 in Table 3.2. It should be noted that all these trials use the same standard PSO operations with the same parameters. Since version 4 that uses 2000 particles is promising in terms of the obtained maximum values in both optimizations at $\theta = 0$ and $\theta = 15$ degrees, the number of particles is chosen as 2000 for the other PSO versions. Different techniques to apply inertia weight parameter are examined in versions 7 to 11. Versions 7, 8 and 9 decreases w as the iterations progress in order to increase the convergence to optimal regions by preventing over-flights from promising areas of the problem space. In these versions, different intervals are chosen for w , i.e., version 7, 8, 9 use $[0.7, 0.1]$, $[1, 0.1]$ and $[0.7, 0]$, respectively. Version 10 uses exactly opposite

Table3.2: Summary of the Examined PSO Versions and Their Applications to a 10×10 Array

PSO Version	w	c_1	c_2	Population	$\theta = 0$ Max	$\theta = 0$ Mean	$\theta = 15$ Max	$\theta = 15$ Mean
1	0.4	2	2	200	126.4	86.83	49.89	34.05
2	0.4	2	2	500	142.0	107.3	53.84	46.47
3	0.4	2	2	1000	140.9	82.8	72.70	52.10
4	0.4	2	2	2000	138.5	88.73	77.02	56.12
5	0.4	2	2	2500	146.6	119.7	61.49	48.45
6	0.4	2	2	5000	138.1	91.92	52.16	43.90
7	0.1-0.7	2	2	2000	145.6	98.34	79.49	60.17
8	0.1-1	2	2	2000	145.6	97.94	70.00	59.12
9	0-0.7	2	2	2000	149.6	93.82	73.88	60.32
10	0.1-0.7	2	2	2000	81.62	58.17	78.90	46.83
11	0.4-0.7	2	2	2000	143.7	107.2	75.85	59.5
12	0.4	2	2	2000	155.0	119.3	78.70	67.16
13	0.4	(0,2)	2	2000	142.1	118.9	65.82	53.92
14	0.4	(0,2)	2	2000	117.8	73.60	73.90	51.52
15	0.4	(0.2)	2	2000	135.5	92.86	67.52	57.47
16	0.4	2	2	2000	52.77	24.18	29.57	20.12
17	0.4	2	2	2000	87.86	62.50	83.55	50.86
18	0.4	2	2	2000	63.26	41.89	60.11	42.18
19	0.4	2	2	2000	142.5	94.76	72.73	61.38
20	0.4	2	2	2000	81.76	67.51	76.76	64.45

idea of version 7, i.e., w is linearly increased in the interval of $[0.1, 0.7]$ rather than decreasing. Unfortunately, this strategy does not work well. Moreover, version 11 chooses w randomly in the region $[0.4, 0.7]$ in order to increase the randomness in the optimization process. These versions (7-11) that select inertia parameter with different techniques indicate that decreasing the inertia weight parameter as the iterations progress improves the performance. Version 12 utilizes the idea of craziness factor. This idea was introduced in [10] and it operates very similar to the mutation mechanism in GAs. Velocity and position vectors of some particles are changed randomly. Similar to the mutation mechanism in GAs, the craziness factor aims to increase the diversity of the explored regions and to prevent early convergences to suboptimal solutions. Among all versions in Table 3.2, version 12 provides the best results. Following this version, versions 13 to 17 focus on the trust and randomness parameters applied with different techniques. It is observed that even a slight change in a single parameter may cause significant reduction in the performance. This is expected because PSO is known to be more sensitive to parameter changes than other evolutionary algorithms [22]. Furthermore, Eberhart and Shi suggested and illustrated that the best choice for trust parameters are constant and 2, and this has become a standard in the PSO literature [12]. Therefore, most of the PSO versions in this study use 2 as both trust parameters. To sum up, the sensitivity of PSO to parameter changes is one of the major challenges to improve its performance. Versions 18 to 20 show the hybrid versions of some promising versions, however the results of the hybrid versions indicate that good approaches together may not lead to better performances since their superior features may disappear when they are hybridized.

3.7 Performance Comparison of GAs and PSOs

Both GAs and PSOs have been widely used in electromagnetic problems [24]. In Figure 3.16, PSO and GA results for directive gain optimizations of the 10×10 array at $(\theta, \phi) = (0, 0)$ are illustrated, as well as the results obtained by the phase-taper method using the array-factor approach [25]. It can be observed

that the GA implementation outperforms the PSO implementation in phase optimizations, where the optimization space contains 2^{700} possibilities. On the other hand, values of the obtained results in on-off optimizations, where the optimization space contains 2^{100} possibilities, are very similar for the GA and PSO implementations. This indicates that PSO is affected negatively when the problem space is enlarged. This is because higher dimensional problems with large optimization spaces often have many identical values and convoluted spaces so that particles can be trapped into local maxima points easily. This situation, which is usually called as premature or early convergence, is one of the major problems in evolutionary algorithms. GAs avoid this phenomenon by utilizing different mutation and selection operators. However, randomness is only added via r_1 and r_2 and maybe via using the craziness factor in PSOs. Thus PSO implementations seem to be more vulnerable for early convergence, as shown in Figure 3.16.

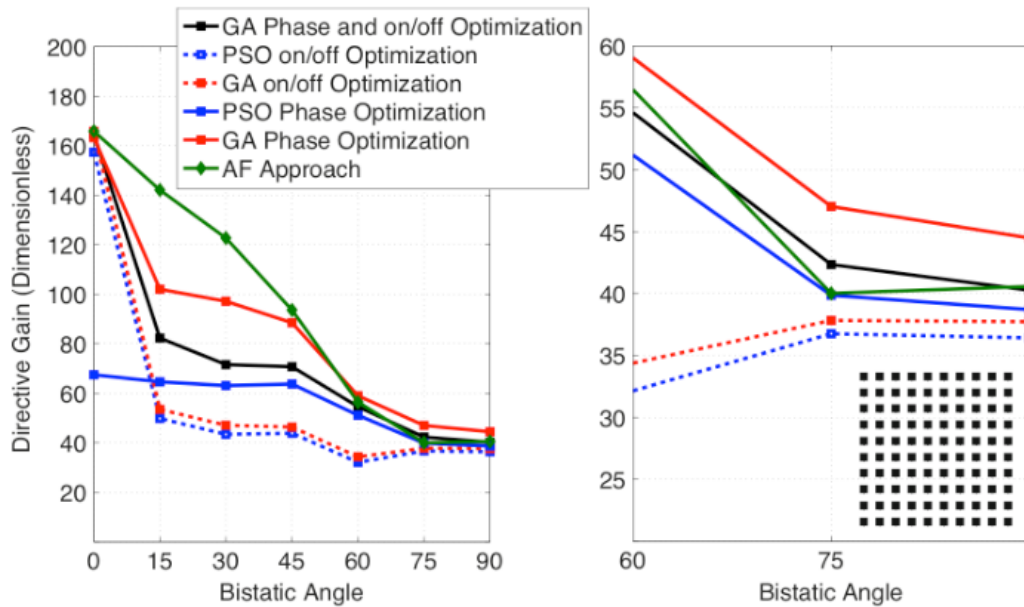


Figure 3.16: Directive gain values obtained via GAs, PSOs, and the phase-taper method. Note that the directive gain values are given in linear scale.

Another observation in Figure 3.16 is that, the phase-taper method provides

higher directive gain values than both GA and PSO implementations at $\theta = 0, 15, 30, 45$ degrees. However, the GA implementation is more successful than the phase-taper method at larger values of θ . This shows that the proposed optimization mechanism may outperform analytical methods based on the array-factor even for a relatively simple and uniform array.

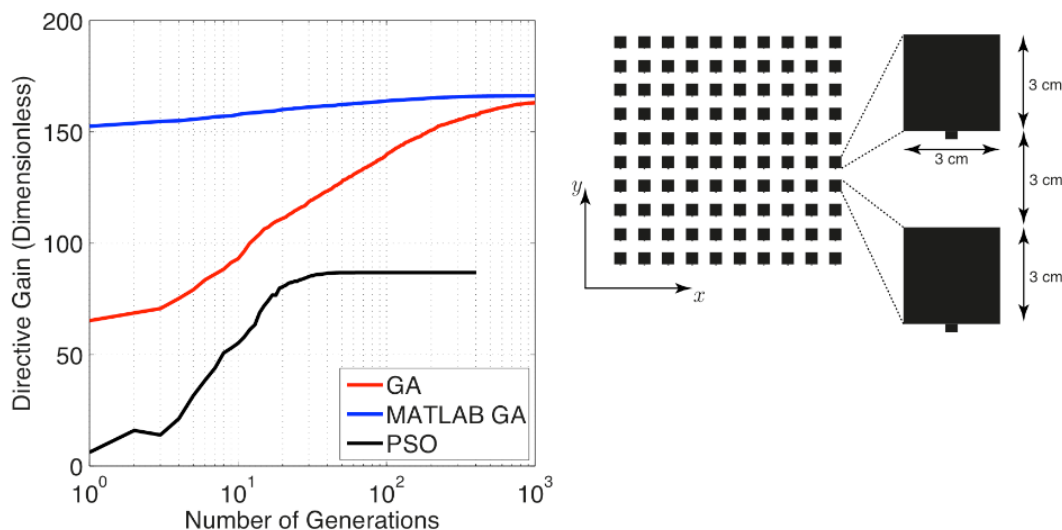


Figure 3.17: Performance comparison of GA, MATLAB GA, and PSO implementations. Note that the directive gain values are given in linear scale.

Another important performance criteria for the optimization methods is the required time for optimizations. In order to observe the performance of the GA and PSO implementations in terms of the processing time, they are compared with the GA tool of MATLAB. For the 10×10 array, GA, MATLAB GA, and PSO implementations complete the optimization in 1000, 5520, and 4982 seconds, respectively, when each algorithm uses a total of 80,000 trials. As depicted in Figure 3.17, the MATLAB GA implementation starts with an initial population that has a very high fitness value, whereas other two in-house algorithms have worse initial populations. In terms of the optimized directive gain values by algorithms, MATLAB GA also yields the best results. However, our GA implementation provides very close results despite it starts with a much

poorer initial population and is almost five times faster than the MATLAB GA. Another observation is that the PSO implementation is trapped to an early convergence and leads to a significantly worse optimization results than the other two implementations.

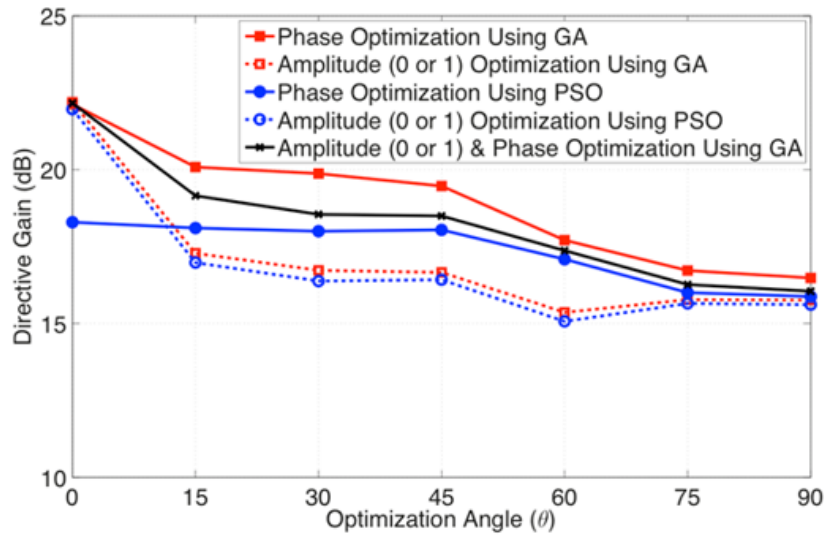


Figure 3.18: Optimized directive gain values for the 10×10 array at 2.45 GHz via different methods.

Directive gain values at different directions obtained by on-off (0 or 1) and phase optimizations using both GA and PSO implementations are illustrated in Figure 3.18. In the same figure, results of full (both phase and on-off) optimizations by the GA implementation are also shown. It can be observed that phase optimizations by the GA implementation provide better results than full optimizations by the same implementation. This may be due to the fact that simultaneous optimizations of amplitudes and phases increase the problem space and decrease the performance of the GA implementation. Radiation patterns obtained via on-off optimizations and phase optimizations using GAs are further illustrated in Figure 3.19 and Figure 3.20, respectively. Steering of the main beam is clearly observed.

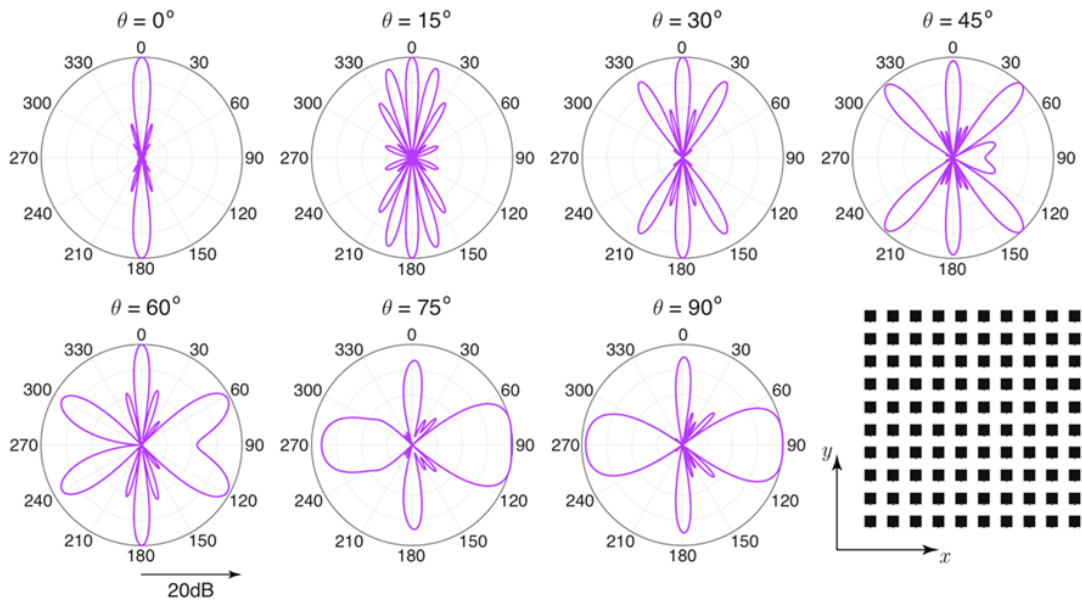


Figure 3.19: Optimized radiation patterns obtained with on - off optimizations via the improved GA.

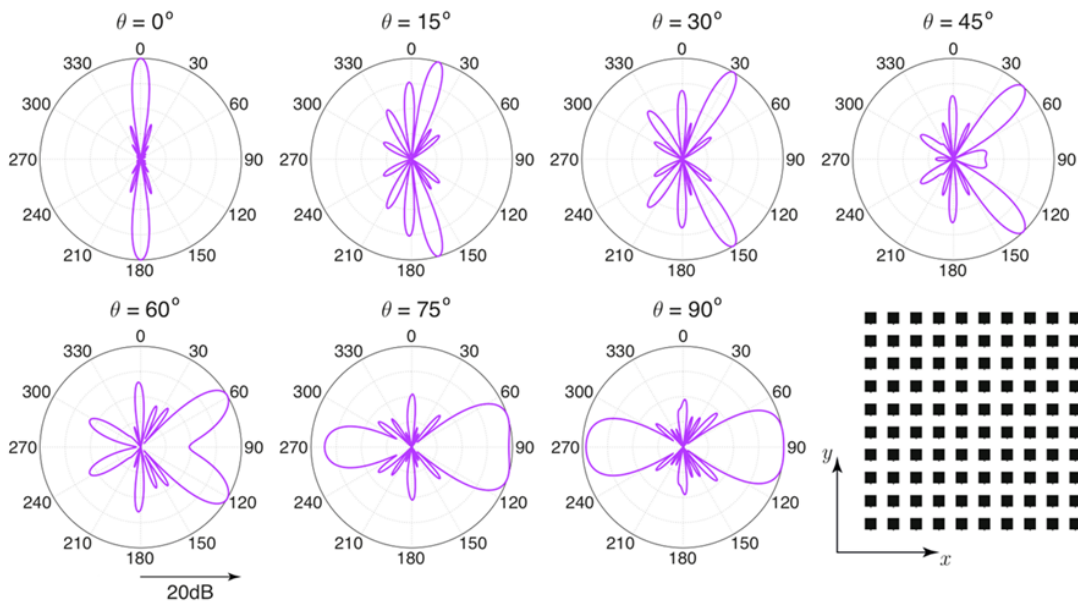


Figure 3.20: Optimized radiation patterns obtained with the phase optimization via the improved GA.

3.8 Multi-Objective Optimizations

One of the major advantages of the proposed optimization mechanism is its convenience to allow for optimizations with different cost functions without requiring a significant change in the optimization code. Only the fitness function should be adjusted according to the optimization purpose. While the results up to this section are related to the optimization of the directive gain, this section presents examples to multi-objective optimizations of arrays. We mainly focus on dual-band optimizations and shaping radiation patterns.

3.8.1 Dual-Band Optimizations

In this section, dual-band antenna arrays and their optimizations via heuristic algorithms, particularly, GAs and PSO methods are considered. Figure 3.21 depicts a test array that consists of patch antennas of different sizes depending on the target frequencies i.e., 2.45 GHz and 5.8 GHz. In many advanced systems, such as radars, it is desirable for arrays to provide multi-band operations with reduced mass and size. The size reduction can be achieved by using dual-frequency array antennas with shared apertures. Moreover, beam scanning in desired directions can be achieved in these dual-band arrays via excitation optimizations [26]. As an important advantage, the developed optimization environment in this study allows for multi-band optimizations, where radiation characteristics at multiple frequencies are considered and optimized simultaneously for multi-band applications.

The optimization procedure is same as the one used for the previous optimization problems, such as 5×5 and 10×10 arrays. The developed GA structure is used for each optimization. Complex far-field patterns at both operation frequencies are calculated and stored in the setup stage. The fitness function is adjusted by considering both frequencies. For example, the fitness function can be taken as the total of the directive gains at the desired direction at 2.45 GHz and 5.80 GHz.

In order to measure the performance of GAs for dual-band optimizations, we first consider single-frequency optimizations at both 2.45 GHz and 5.80 GHz. Cost

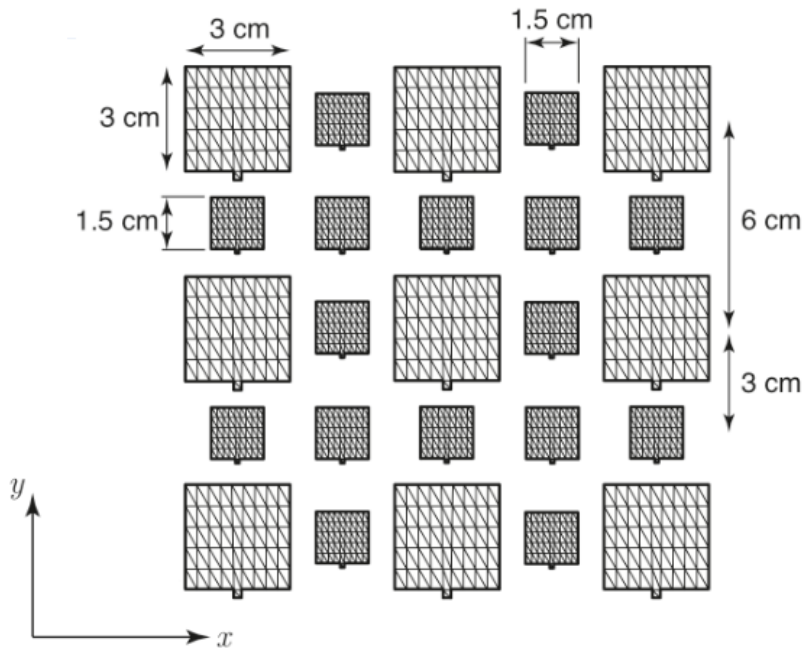


Figure 3.21: Geometry of a dual-frequency array operating at 2.45 GHz and 5.8 GHz.

function with respect to the number of generations can be seen in Figure 3.22 and Figure 3.23, respectively, for single-frequency optimizations at 2.45 GHz and 5.80 GHz.

Figure 3.24 presents the directive gain values obtained when the optimizations are performed at single frequencies (2.45 GHz and 5.80 GHz) and simultaneously at both frequencies. In the single frequency optimizations, only the results obtained for the considered frequency are depicted, as the values for the other frequency are very low. Considering the dual-frequency optimizations, directive gain values naturally drop in comparison to single-frequency optimizations. However, the dual-frequency optimizations maintain high directive gain values simultaneously at both frequencies. Specifically, the dual-frequency optimizations improve the sum of the directive gain values at 2.45 GHz and 5.80 GHz, in comparison to single-frequency optimizations that are improving the directive gain at a single frequency while completely neglecting the other frequency. The results obtained via the phase-taper method are also illustrated in Figure

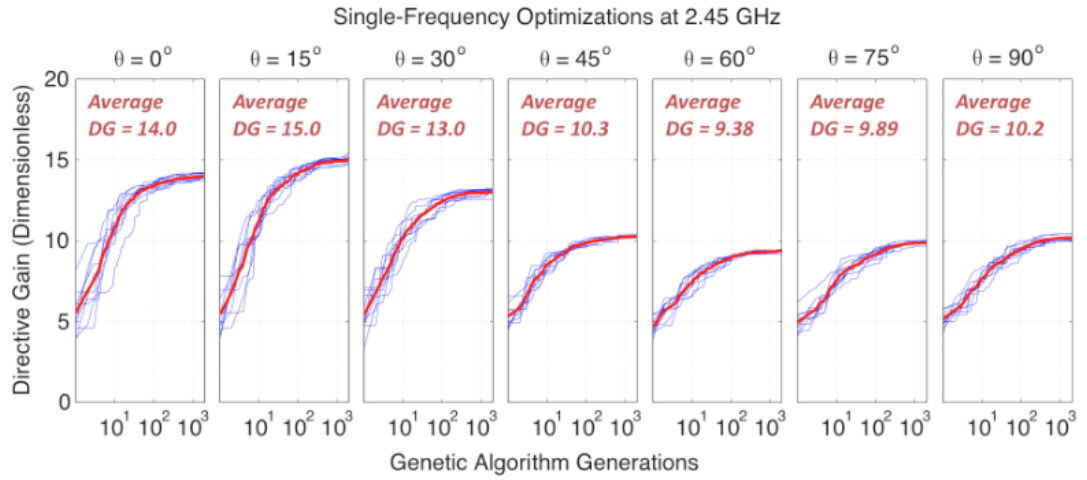


Figure 3.22: Cost functions with respect to the number of generations when the improved GA implementation is used to maximize the directive gain in various directions at 2.45 GHz. Note that the directive gain values are given in linear scale.

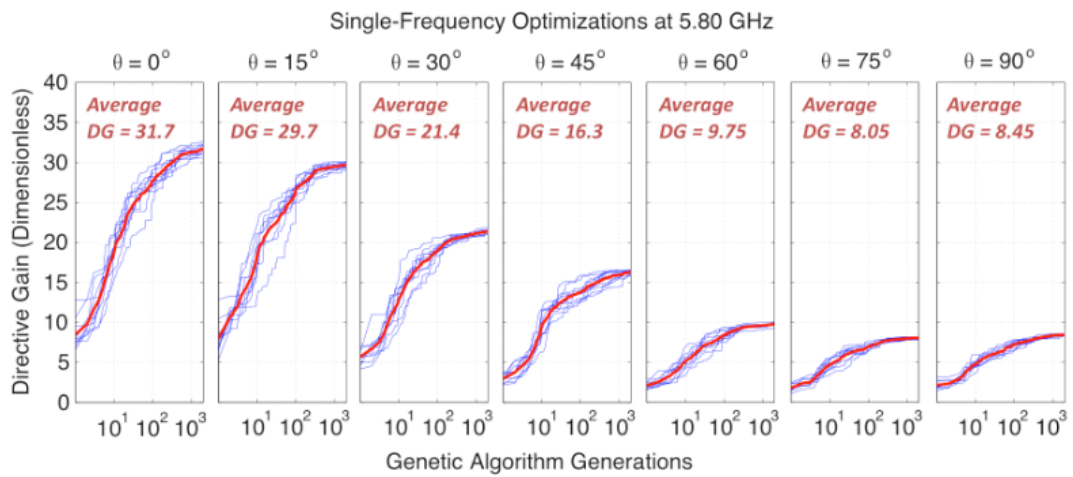


Figure 3.23: Cost functions with respect to the number of generations when the improved GA implementation is used to maximize the directive gain in various directions at 5.80 GHz. Note that the directive gain values are given in linear scale.

3.24. It can be seen that GA outperforms the optimal results of the phase-taper method at each angle. This is a natural consequence of short distances between array elements, leading to strong mutual couplings. Radiation patterns at 2.45 GHz and 5.80 GHz that are obtained by the dual-band optimizations with GAs can be seen in Figure 3.25 and Figure 3.26, respectively.

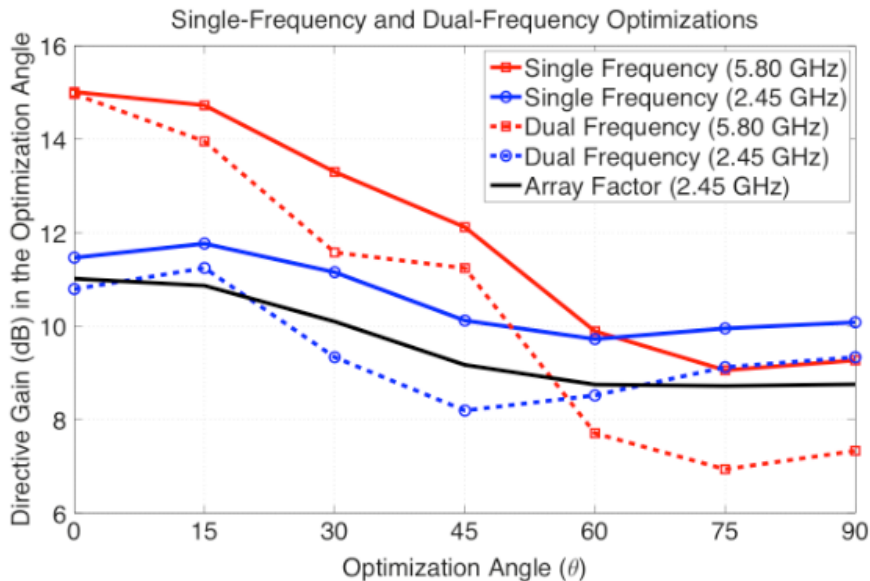


Figure 3.24: Optimized directive gain values for the dual-frequency array in Figure 3.21.

3.8.2 Shaping Radiation Patterns

Reduction of side-lobe levels is a popular application in array optimization problems [27], [28]. In order to show that the proposed mechanism can be used for such optimizations, the 10×10 array is optimized for maximizing the directive gain at two different directions, i.e. $\theta = 0$ and 30 degrees, while setting a sharp threshold for the side lobes. The results obtained with GAs are depicted in Figure 3.27. It is seen that the optimization achieves high directive gain values at the desired directions, while preventing side lobes from exceeding the threshold.

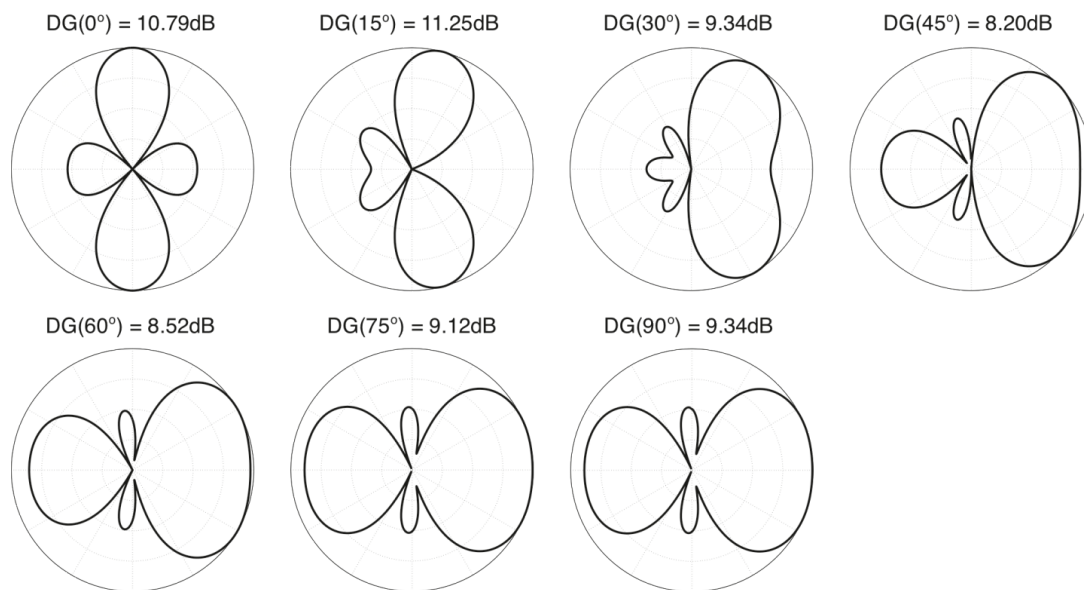


Figure 3.25: Radiation patterns obtained by dual-frequency optimizations of the array in Figure 3.21 at 2.45 GHz.



Figure 3.26: Radiation patterns obtained by dual-frequency optimizations of the array in Figure 3.21 at 5.80 GHz.

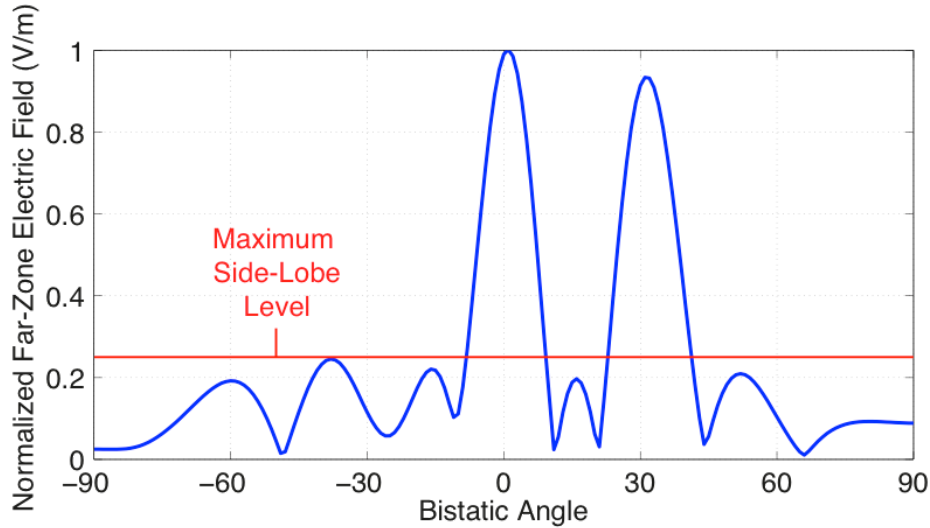


Figure 3.27: Normalized far-zone electric field obtained via the GA for maximizing the directive gain simultaneously at $\theta = 0$ and 30 degrees while setting a threshold for the side lobes.

3.9 Remarks

In this chapter, the excitation optimizations of three different array geometries are demonstrated. Some of the underlined points in this chapter can be listed as follows.

- The superposition principle is utilized to reduce the number of current-density computations to the number of array elements, without omitting mutual couplings.
- Improvements on GA operations are achieved via alternative techniques such as success-based mutation operation, family elitism, and one-by-one crossover.
- Various versions of GAs and PSOs are examined and their performances are discussed.
- Multi-objective optimizations of the arrays with different cost functions are shown.

In the next chapter, we consider geometry optimizations of pixel antennas.

CHAPTER 4

GEOMETRY OPTIMIZATIONS OF PIXEL ANTENNAS

4.1 Introduction

Optimizations of antenna geometries, especially when they involve structural changes, are challenging because each different geometrical configuration corresponds to a new electromagnetic problem that requires to be solved accurately [29]. Moreover, optimization spaces for such problems can be extremely large [30]. While gradient-based optimizers [31] may be preferred due to their fast convergence characteristics, heuristic algorithms provide flexibility in design and optimization procedures. Therefore, combining heuristic algorithms with full-wave solvers for optimizations of antenna geometries are very popular in the literature. For the geometry optimizations of antennas, GAs [32], PSOs [33] and simulated annealing algorithms [34] with different full-wave solvers, such as the method of moments [35] and the finite-difference time-domain method [36], are examined in the literature. These studies point out the advantages of the heuristic algorithms as well as their drawbacks. The main advantage of these algorithms is their ability to cover extremely large optimization spaces with flexible cost functions [37]. On the other hand, they may not guarantee a convergence to acceptable results in constant or predefined response times. This especially limits the usage of these algorithms in real-time applications.

4.2 Optimization Mechanism

Similar to the excitation optimizations, our optimization mechanism is a combination of GAs and MLFMA. Binary-coded parameters are very appropriate to apply on geometry optimizations where each portion of an antenna can be represented with a single bit. For a suggested antenna configuration by the GA optimizer, the required portions are disconnected by removing the related RWG functions, while all other coefficients are found by an iterative solution accelerated with MLFMA. This mechanism allows for removing desired portions of the geometry rapidly. Although the geometry optimizations of antennas by removing portions or shorting strips between antennas and ground planes are known in the literature [38], this study is different from port-based approaches where antenna problems are solved and replaced via equivalent ports before optimizations [39]. It should be underlined that in our mechanism, each trial suggested by GA is solved via a full-wave solver. Therefore, the proposed mechanism may be used for different structures including antennas with other parasitic objects.

4.2.1 Lookup-Table Concept

Since GAs may demand thousands of trials for optimizations, it is crucial to increase their efficiency by reducing the number of full-wave trials. When populations formed in each generation are examined, it can be seen that a GA often requests the evaluation of the same configurations. It is obvious that storing the evaluated configuration and its corresponding fitness value in a table may save significant time by avoiding multiple evaluations. For that purpose, a lookup table is utilized. Figure 4.1 illustrates the number of calls of a lookup table during the optimization of the directive gain of a cage-dipole antenna at various directions. In these optimizations, 20 individuals and 200 generations are used, hence a total of 4000 trials are allowed per optimization process. It is seen that almost a quarter of these trials are taken from the lookup table in these six different optimizations, proving that the lookup table saves significant time.

A lookup table can be considered as the memory of an optimization because it

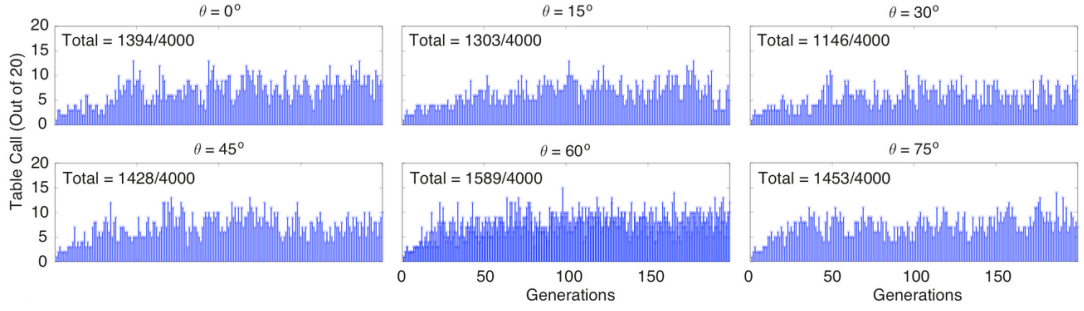


Figure 4.1: Numbers of lookup table calls in GA optimizations of the directive gain of a cage-dipole antenna at various directions.

stores all desired parameters as the optimization continues. This provides the designer a dynamic control ability over the optimization. For example, mutation rates and crossover operations can be changed dynamically when a superior individual dominates the pool. Even though the dynamic control over GAs is a promising concept [40], this study focuses on the dynamic control over the full-wave solver part since it is the actual bottleneck in antenna optimizations.

4.3 Fabrication of Inkjet Antennas

Optimized antennas are printed on photograph papers using silver toner in standard commercial printers (Epson). Although inkjet printing via commercial printers is inexpensive and enables printing tiny details, it involves some challenges, such as maintaining the conductivity uniform over the antenna surfaces. Furthermore, the effects of the used photo papers and silver-based toners, as well as the life time of printers should also be considered. As it is well known in the literature [41], inkjet antennas need to be cured after printing, especially when standard printers are used. Main reason is that inkjet printers are not designed for consistency, i.e., uniformity of the ink, but designed only for printing readable patterns. In order to maintain a uniform conductivity over antenna surfaces, a simple oven is used to cure the printed antennas. It should be noted that the curing temperature and duration are very critical for producing high-quality printouts with high conductivity all through the antenna. Figure 4.2

shows the results of some curing trials for a structure that is produced to observe the effects of curing on resistance. The average resistance values of the samples are measured via a DC multimeter and plotted with respect to the curing duration. It is seen that temperatures over 100°C lead to significant drops in the resistance while the duration becomes less effective when the temperature is high. It should be noted that temperatures above 200°C deforms the photograph paper hence it is not shown in these trials. The effect of the temperature on the prints is also visible in the zoomed photographs. According to these observations, produced inkjet antennas are cured for one hour at 175°C since it provides good conductance in a relatively shorter time than other trials. It may be beneficial to underline the fact that curing must be applied immediately after the inkjet printing.

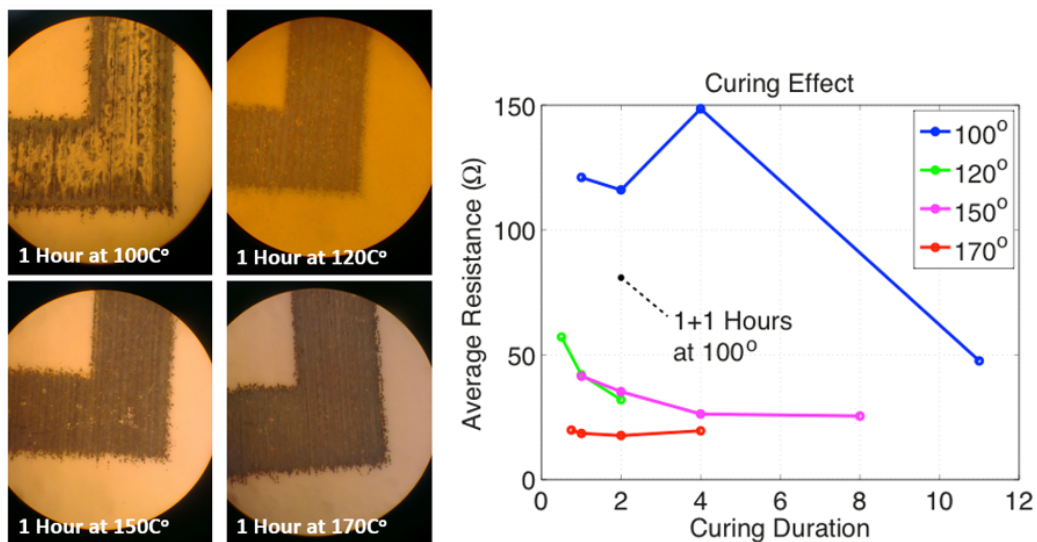


Figure 4.2: Cured samples of inkjet prints and the dependency of the resistance to the curing duration and temperature.

Another important issue regarding the production of inkjet antennas is the selection of the paper type, which possesses a significant role for the quality of the antennas. Since heat-curing is crucial when standard printers are used to produce the antennas, the paper substrates should be resistant to high tem-

peratures. Unfortunately, many photograph or transparent papers with high plasticity tend to be bend or deformed above 100°C hence damage the silver print. On the other hand, papers with low plasticity can be very absorbent which leads to defective prints with small cracks preventing the conductivity over antenna surfaces. Therefore, there are only few commercial photograph paper types that are appropriate for antenna printing. Based on numerous trials of different combinations, Canon GP-501 photograph paper and silver based toner of Novacentrix JS-B25P are used in this study. Finally we note that, the life time of the commercial printers are another issue for inkjet printing. Since silver-based toners cause oxidization in the printer heads, the quality of the produced antennas drop significantly as the printers are used. Therefore, the printers are replaced frequently to maintain high quality prints.

4.4 Optimizations of Cage-Dipole Antennas

In this section, full wave optimizations of an inkjet dipole antenna with cage shape is presented. The overall size of the antenna geometry is $3.2\text{ cm} \times 6.8\text{ cm}$ and it involves 80 gap locations as shown in Figure 4.3. It should be noted the antenna is fed from its center. In order to achieve the desired input and radiation characteristics, some of these gap locations are opened (disconnected) as a result of the optimization. The proposed antenna geometry has a potential to yield various types of antenna structures with the proper adjustment of these connections. A total of 80 gap positions, which are on the two arms of the antenna, are adjusted symmetrically which corresponds to an optimization space with $2^{40} \approx 10^{12}$ unique configurations. Therefore, each individual in GA populations has a chromosome of 40 bits where each bit represents two symmetric gap locations. It is observed that GAs provide satisfactory optimizations in less than 4000 trials, each of which corresponding to a full-wave solution.

Different optimization goals are tried in order to see the capabilities of the proposed antenna geometry as well as the optimization mechanism. Figure 4.4 depicts simulation results of optimized antenna configurations when the optimization goal is to maximize the directive gain at different directions at 5.80 GHz

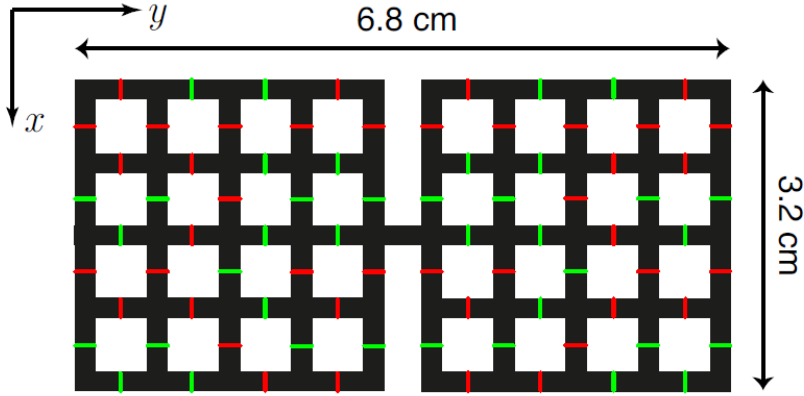


Figure 4.3: Geometry of the cage-dipole antenna and gap locations. An optimized configuration is shown, where green and red colors represent short circuit (no gap) and open circuit (gap), respectively.

(in free space). It can be seen that the proposed geometry is capable of changing the maximum directive gain at different angles via proper selections of its connections.

Since the cage-dipole antenna has promising capabilities, two different optimization criteria are chosen where the purposes are to increase the directive gain at $(\theta, \phi) = (0, 0)$ and $(\theta, \phi) = (90, 0)$, respectively, while matching the antenna input impedance to 50Ω at 5.80 GHz. While the antennas are printed on photograph papers, our initial experiments show that their exact modeling with very thin and finite dielectric layer is not essential. Therefore, in order to include the dielectric effects of the photograph paper, a homogeneous medium with a relative permittivity of approximately 4.5 is used. The cost function, which is the fitness function of GAs, is defined as

$$CF(\theta_0, \phi_0) = (1 - |\Gamma|)D(\theta_0, \phi_0) \quad (4.1)$$

where $D(\theta_0, \phi_0)$ is the directive gain in a given direction (θ_0, ϕ_0) and Γ is the reflection coefficient defined as

$$\Gamma = \frac{Z_{in} - Z_o}{Z_{in} + Z_o}. \quad (4.2)$$

In (4.2), Z_{in} is the input impedance of the antenna, while Z_o is the impedance

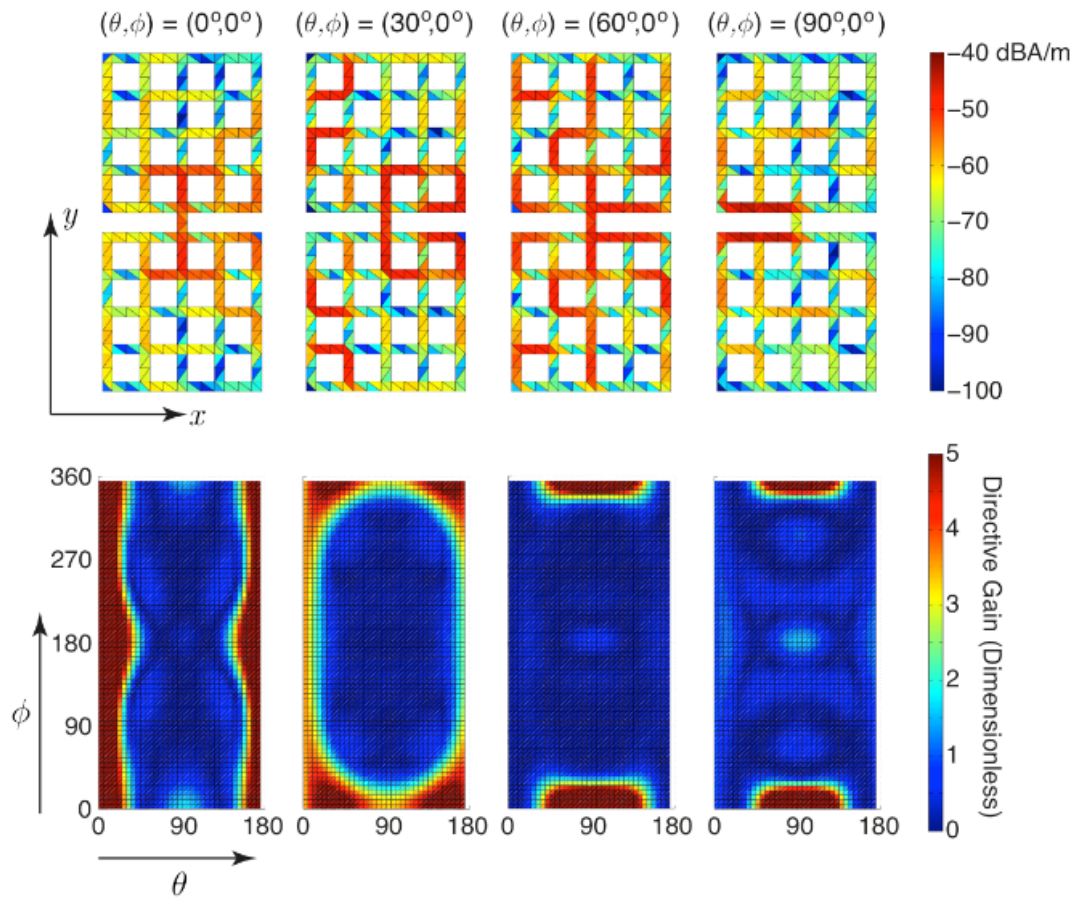


Figure 4.4: Simulated current distributions and directive gain plots of optimized cage-dipole antennas.

of the port/device matching to the antenna. In this study, we choose $Z_o = 50\Omega$. Each optimization is carried out ten times and the obtained results are listed in Table 4.1 and Table 4.2.

Table4.1: Simulation Results of Optimized Antennas For $(\theta, \phi) = (0, 0)$

Optimization No	Input Impedance	Power Reflection Coefficient (dB)	Directive Gain (0,0)	Cost Value
1	50.66 - 0.623i	-40.92	6.1	6.04
2	54.69 + 2.510i	-25.88	5.35	5.08
3	43.68 + 12.32i	-16.68	7.60	6.49
4	42.75 - 5.849i	-19.98	6.91	6.22
5	49.91 - 0.820i	-41.68	5.72	5.68
6	49.76 - 3.849i	-28.26	7.24	6.96
7	55.57 + 4.784i	-23.26	7.94	7.38
8	49.24 - 3.072i	-29.92	4.90	4.74
9	48.60 + 11.16i	-18.91	6.10	5.41
10	92.27 - 40.49i	-8.05	6.91	4.17

The results in Table 4.1 and Table 4.2 indicate that there are various antenna configurations that provide desired characteristics. The first optimization in Table 4.1 and 6th in Table 4.2 are selected for further analysis. The configurations of the selected antennas and their simulation results are shown in Figure 4.5.

Figure 4.6 illustrates the cost function and the number of usages of the lookup table with respect to the generations of GAs for the first optimization in Table 4.1. It can be observed that GAs increase the cost function from a very low value to satisfactory levels. Furthermore, the lookup table proves its importance to minimize the required optimization time since GAs use it extensively. Another important issue is the existence of naturally occurring parasitic parts that are created during GA optimizations. The effects of these parasitic parts should be calculated accurately because they have a significant effect on the overall radiation characteristics of the antennas. Figure 4.7 shows the power reflection coefficient results for both an optimized configuration and the one without the parasitic parts.

Table4.2: Simulation Results of Optimized Antennas For $(\theta, \phi) = (90, 0)$

Optimization No	Input Impedance	Power Reflection Coefficient (dB)	Directive Gain (90,0)	Cost Value
1	66.02 - 17.45i	-13.90	11.56	9.23
2	49.63 + 6.957i	-23.12	12.17	11.3
3	60.08 - 5.723i	-19.56	8.73	7.82
4	59.05 + 9.230i	-18.56	10.25	9.04
5	55.69 + 2.829i	-24.42	9.52	8.95
6	51.37 + 1.596i	-33.66	10.40	10.2
7	49.30 + 2.561i	-31.46	10.19	9.91
8	46.96 + 9.022i	-20.20	8.61	7.77
9	41.89 - 22.11i	-12.07	11.14	8.37
10	54.03 - 5.061i	-24.14	11.67	11.0

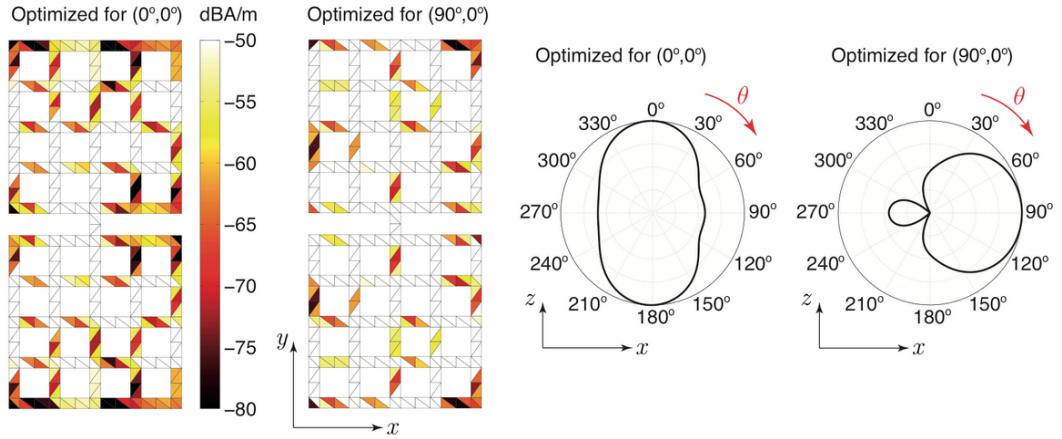


Figure 4.5: Two optimized antenna configurations. Induced currents on the antennas as well as radiation patterns on the $z - x$ plane are depicted.

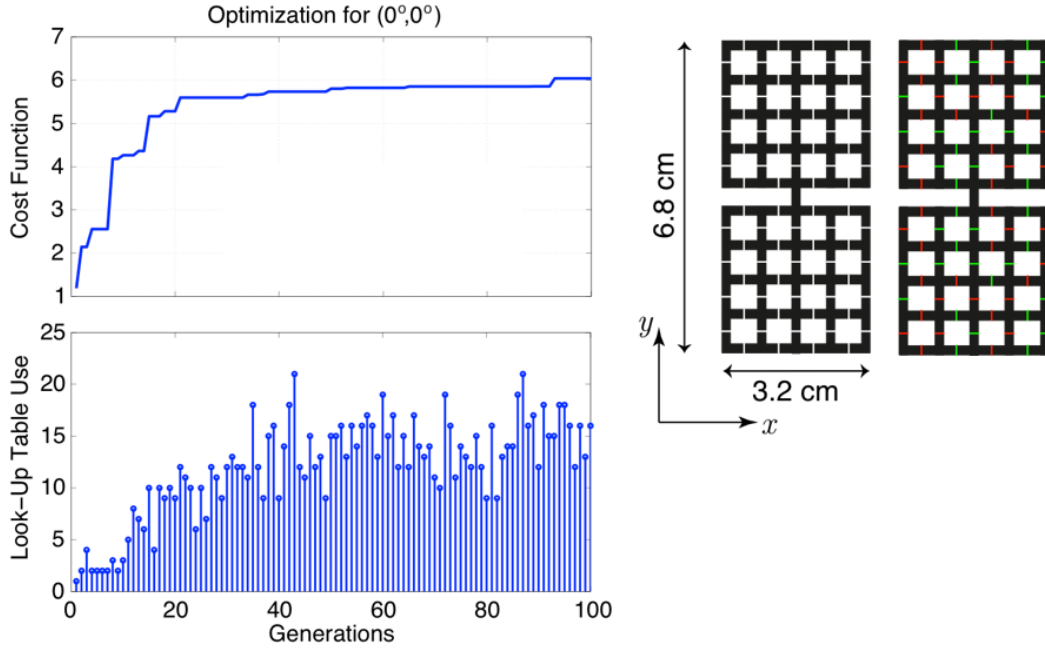


Figure 4.6: Optimization of the antenna structure depicted in Figure 4.3 to maximize the cost function in Equation (4.1) for $(\theta, \phi) = (0, 0)$. Both the cost function value and the number of table usages are plotted with respect to generations.

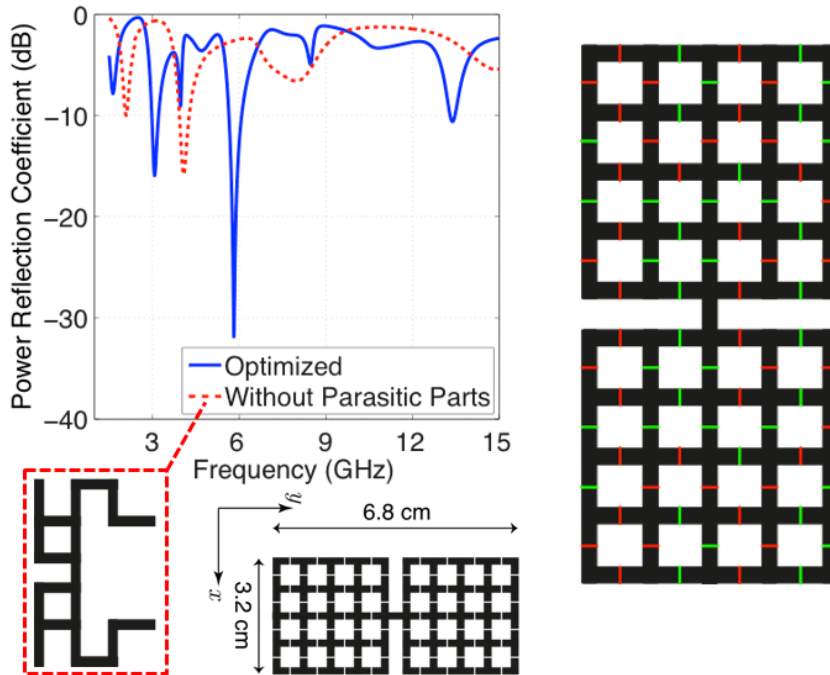


Figure 4.7: Power reflection coefficient (dB) for both an optimized configuration and the one without naturally occurring parasitic parts. Note that the simulation results are obtained in free space at 5.8 GHz.

After the optimizations, one of the antennas is printed using silver-based toners in commercial printers and cured in order to maintain conductivity over the antenna surface. Antenna is attached to a coaxial end using a conductive epoxy and the power reflection coefficient is measured. A comparison of the measured and simulated values can be seen in Figure 4.8. It should be noted that the simulation result in Figure 4.8 is obtained by using a dielectric host medium with $\epsilon_{eff} = 4.5$ to account the effects of the paper substrate. It can be seen that both simulation and measurement results agree on the frequency where the minimum value of the power reflection coefficient is observed.

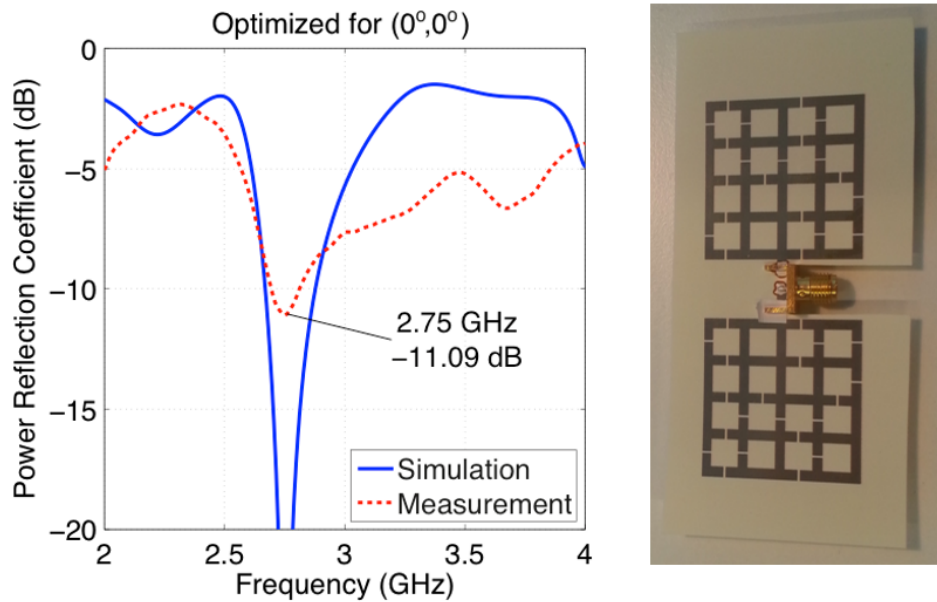


Figure 4.8: Measured and simulated power reflection coefficient values for the optimized antenna.

Finally, in order to compare the simulation results with a commercial software, an optimized antenna is implemented and simulated in HFSS. Figure 4.9 shows the simulation results obtained via HFSS for the optimized antenna when the permittivity of the substrate is given as 4.5. Although, there are some differences between MLFMA and HFSS results, they both have low values for the power reflection coefficient at around similar frequencies, i.e., 2.75 GHz and 2.5 GHz.

In addition, both simulations illustrate that the antenna radiates toward $(\theta, \phi) = (0, 0)$ at the frequency of interest. (See Figure 4.5 for comparison.)

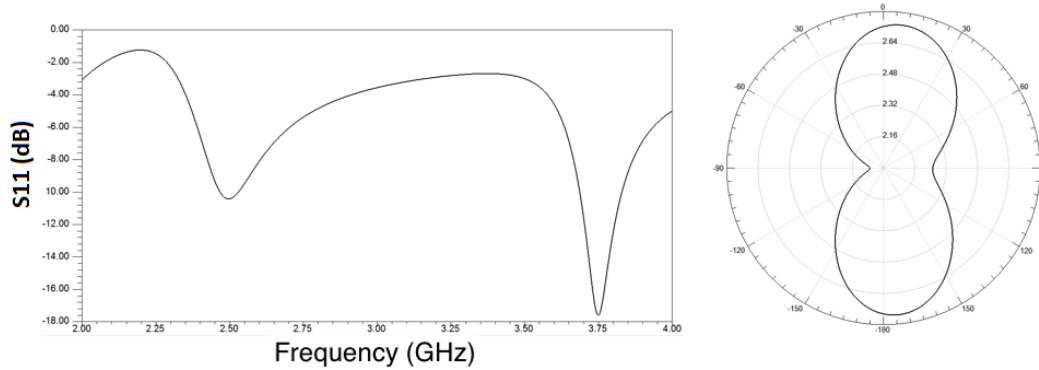


Figure 4.9: S_{11} and radiation plots obtained via HFSS.

4.5 Optimizations of Patch-Pixel Antennas

Figure 4.10 shows the geometry of a type of pixel antennas considered in this work. The antenna consists of two metallic patches of size $4.14 \text{ cm} \times 5.68 \text{ cm}$ that are combined with 0.508 cm distance (the thickness of two photograph papers) between them. The main purpose of the optimization is to determine the triangular pixels to be removed from the top layer in order to achieve desired radiation and input characteristics at 3.2 GHz that corresponds to the frequency band for WiMAX [42]. It should be noted the triangle pixels are exactly matching to the triangles that are used in the discretization for numerical solutions with MLFMA. Proposed antenna has many details which make its production via inkjet printing advantageous since inkjet printing is appropriate to produce tiny details even better than large areas.

There are 320 triangles on the top layer of the antenna and each triangle is represented via single bit in the chromosome of the individuals in GAs. Total of 10,000 trials are used for the optimization process. Two different optimizations are carried out for this antenna where the main purpose is to maximize the

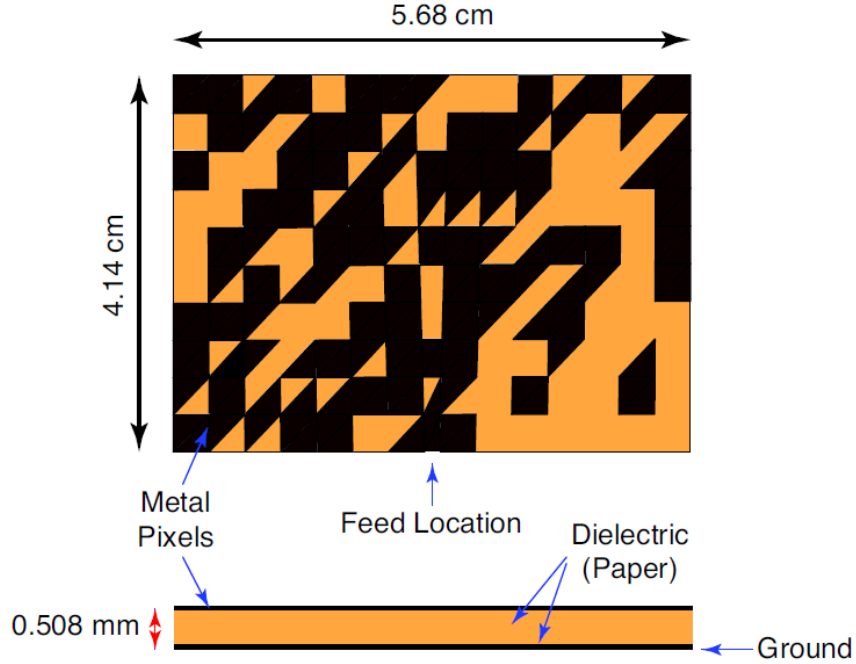


Figure 4.10: Geometry of an optimized patch-pixel antenna.

antenna gain (cost function) at $(\theta, \phi) = (0, 0)$ and $(\theta, \phi) = (30, 0)$ at the desired frequency. Various pool sizes are examined, and the cost functions with respect to the number of generations are illustrated in Figure 4.11 and Figure 4.12. The best results with the highest cost functions for these two optimization sets are shown in Figure 4.13 and Figure 4.14. It can be observed that various configurations of the proposed antenna geometry may provide the desired characteristics.

The optimizations for $(\theta, \phi) = (30, 0)$ may be more challenging than the optimizations for $(\theta, \phi) = (0, 0)$, and this may be observed in Figure 4.11 and Figure 4.12. The optimized antennas for $(\theta, \phi) = (30, 0)$ are examined in more detail, fabricated and measured. Simulated radiation pattern of an optimized antenna for $(\theta, \phi) = (30, 0)$ is shown in Figure 4.15, where normalized far-zone electric field intensity is plotted with respect to the bistatic angle on the $z - x$ and $z - y$ cuts. The figure also shows the geometry of the antenna as a result of the optimization. While the optimization aims to provide maximum radiation in

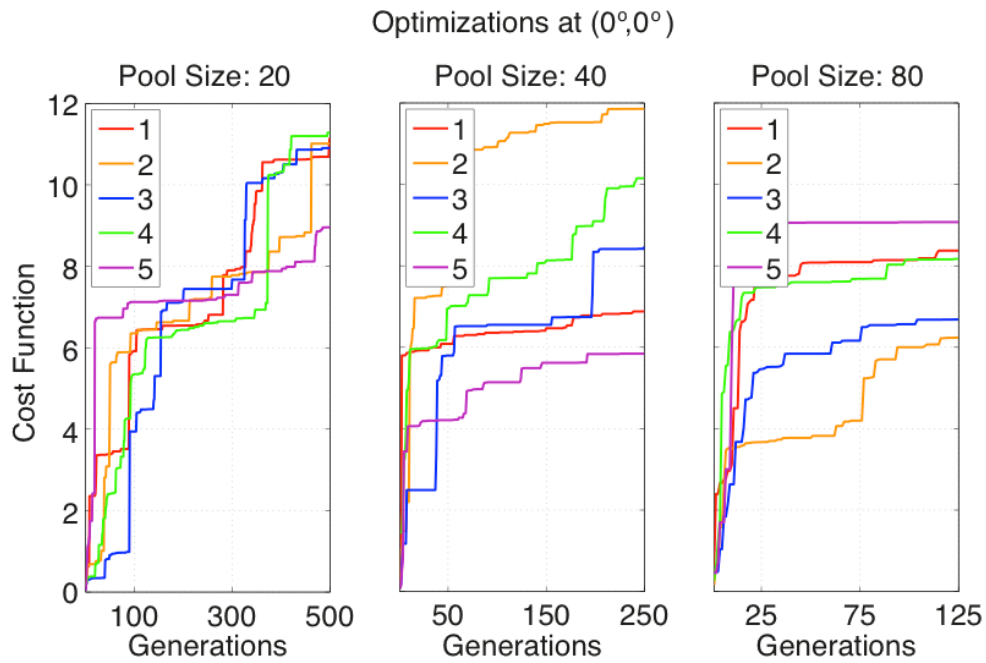


Figure 4.11: Cost functions with respect to the number of generations of the optimizations for $(\theta, \phi) = (0, 0)$.

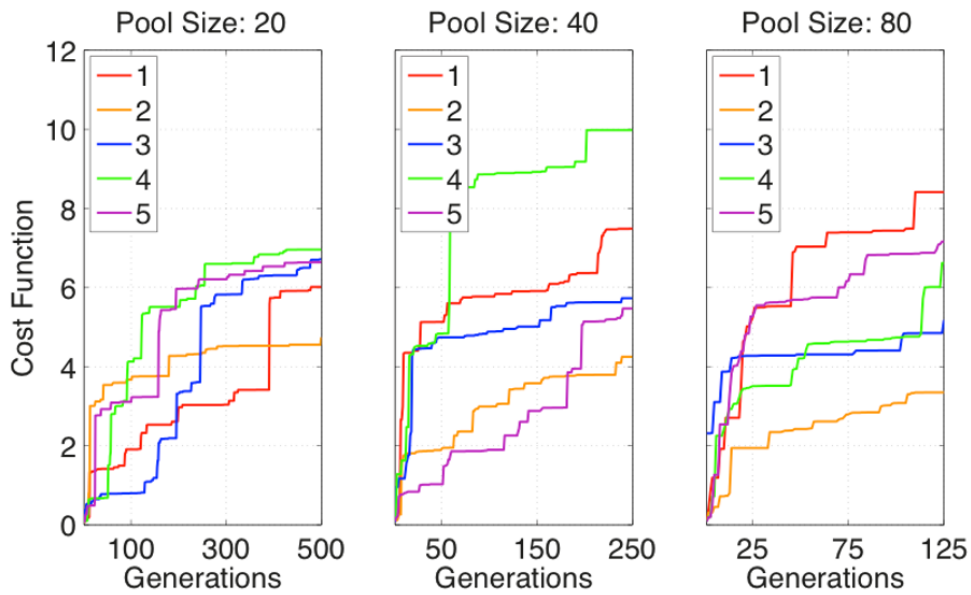


Figure 4.12: Cost functions with respect to the number of generations of the optimizations for $(\theta, \phi) = (30, 0)$.

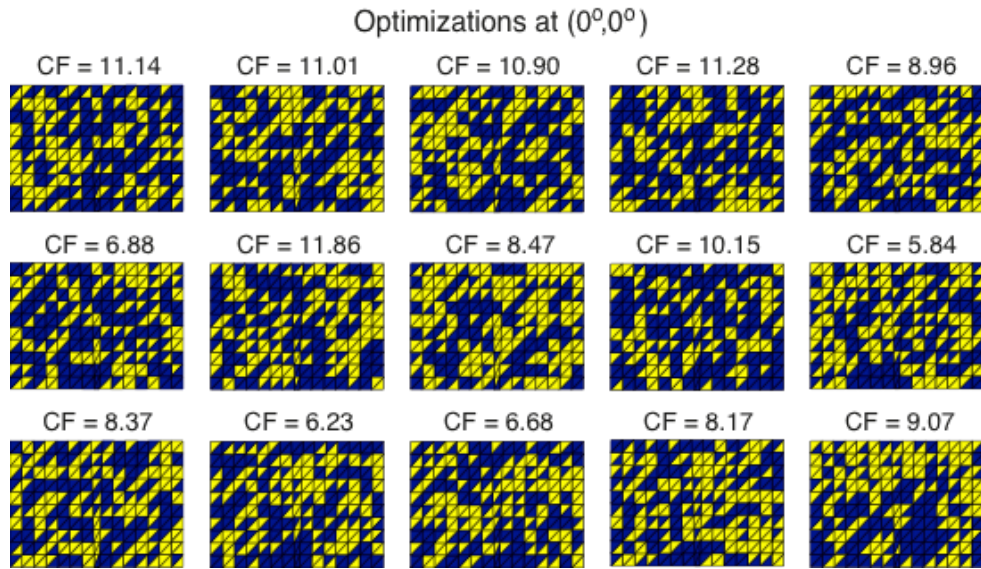


Figure 4.13: Obtained antenna configurations of the optimizations for $(\theta, \phi) = (0, 0)$.

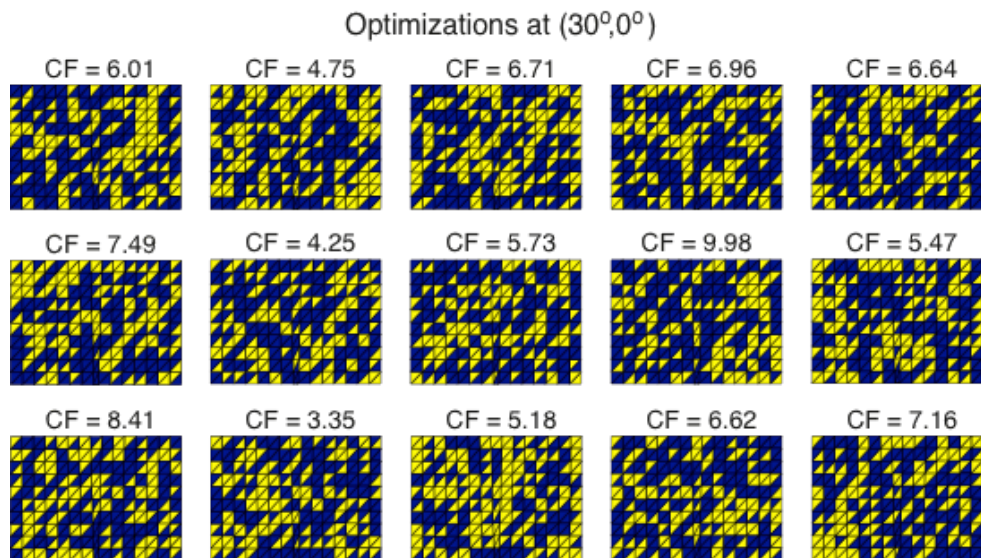


Figure 4.14: Obtained antenna configurations of the optimizations for $(\theta, \phi) = (30, 0)$.

the $(\theta, \phi) = (30, 0)$ direction, a maximum radiation occurs at 21 degrees, which is acceptable.

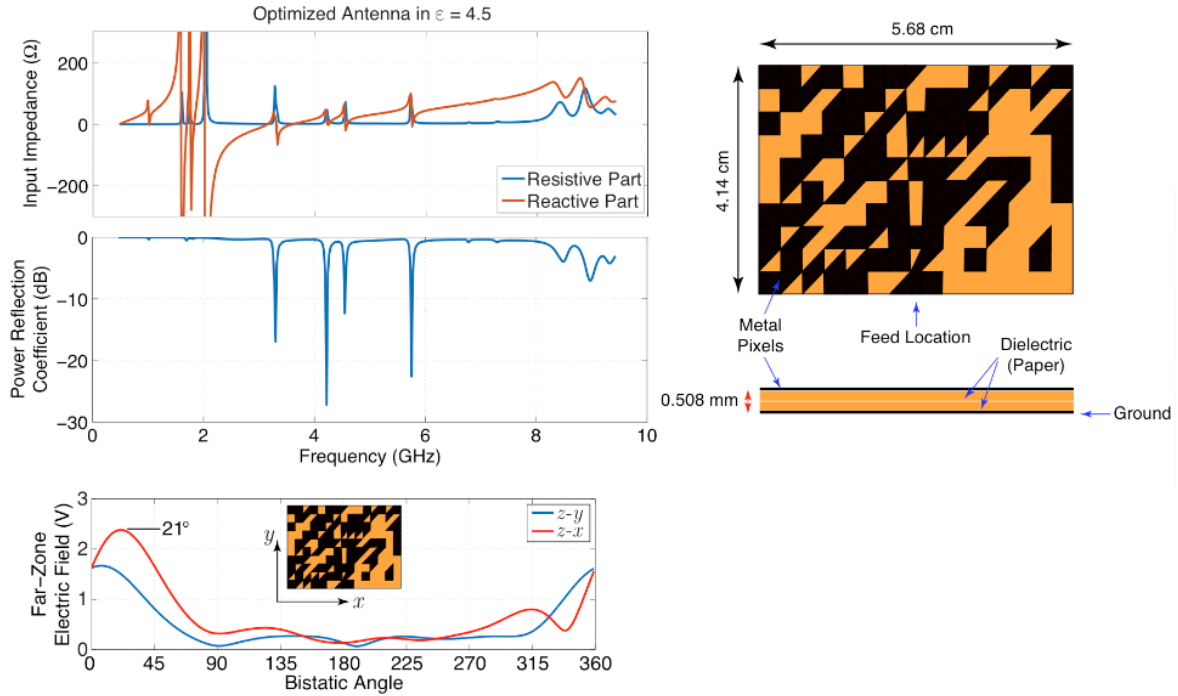


Figure 4.15: Far-zone electric field radiated from the optimized antenna simulated with MLFMA. The geometry of the antenna is also shown.

The optimized patch-pixel antenna is produced via inkjet printing and measured. Figure 4.15 shows the measured input impedance of the antenna, as well as the power reflection coefficient when the antenna is connected to 50Ω . It is observed that the power reflection coefficient has a minimum with a value of -32.48 dB at 3.196 GHz, which is very close to the desired operation frequency.

4.6 Remarks

In this chapter, the geometry optimizations of the cage-dipole and patch-pixel antennas are discussed. Some of the underlined points in this chapter can be listed as follows.

- The lookup table concept, which provides the designer a dynamic control ability over the optimization, is introduced and its effectiveness to reduce optimization times is presented.
- Fabrication of inkjet antennas that are produced by using silver-based toners in commercial printers and associated challenges are briefly explained.
- An efficient way to disconnect required portions in the geometry optimizations by removing the related basis functions is illustrated.
- Numerical and measurement results of the optimized antennas are discussed.

In the next chapter, we consider dynamic accuracy control over optimizations by employing approximate forms of MLFMA.

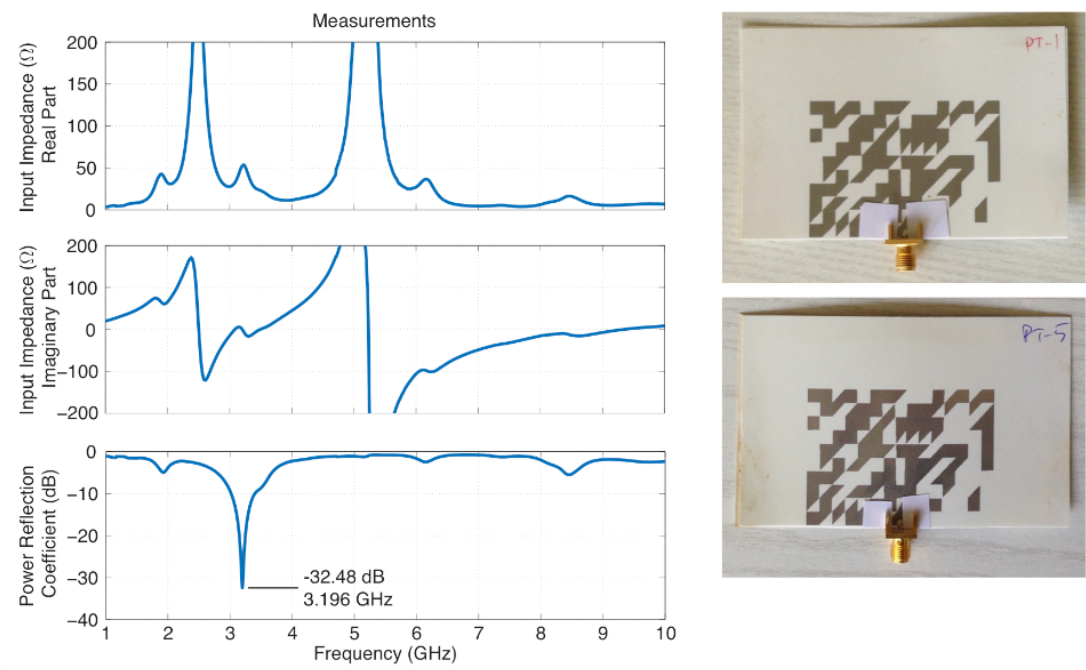


Figure 4.16: Measured input impedance of the patch-pixel antenna and the power reflection when it is connected to 50Ω .

CHAPTER 5

ACCURACY CONTROL BY USING APPROXIMATE FORMS OF MLFMA

5.1 Introduction

Although MLFMA performs matrix-vector multiplications very rapidly, an optimization mechanism utilizing heuristic algorithms may demand thousands of trials. These huge number of trials required in the optimizations make the optimization process overwhelming with excessive computational costs, which may be alleviated by resorting to remodeling the systems under interest in more suitable forms [35]. In this chapter, an alternative mechanism is presented, where full-wave solutions are not reformulated but enhanced with a dynamic and adjustable accuracy control to improve the efficiency of optimizations without sacrificing the quality of results. As an advantage, MLFMA enables error controllability for the solutions. The developed mechanism is based on the fact that accuracy may not be critical for all optimization trials and it can be made an optimization parameter rather than a fixed constraint. A penalty strategy is utilized when solutions with lower accuracy are done in order to maintain a quality threshold of the final results.

5.2 Approximate Forms of MLFMA

The idea behind employing approximate forms of MLFMA, which can be called as approximate MLFMA (AMLFMA), in the optimizations is mainly based on

two observations. Firstly, it is not necessary to solve each trial suggested by heuristic algorithms with the same accuracy. It is known that heuristic algorithms may demand the evaluation of a poor suggestion many times especially at the beginning of the optimization. These less critical trials may be solved with lower accuracy in order to accelerate the optimization. Secondly, MLFMA allows for a dynamic accuracy control that can be used to facilitate accuracy variation through an optimization.

In typical electromagnetic simulations, accuracy of MLFMA is controlled via the excess bandwidth formula [43] that provides the required number of harmonics for a given worst case error. Using a full MLFMA, the cost of an $N \times N$ matrix-vector multiplication can be written as

$$C = c_0 N_{\text{near}} + \sum_{l=1}^L c_l N_l (\tau_l + 1)^2, \quad (5.1)$$

where c_0, c_1, \dots, c_L are constants, $L = \mathcal{O}(\log N)$ is the number of active levels, $N_{\text{near}} = \mathcal{O}(N)$ is the number of near-zone interactions, N_l represents the number of nonempty boxes, and τ_l is the truncation number at level l . In general, $N_1 = \mathcal{O}(N)$, $N_l \approx N_{l-1}/4$ for $l > 1$, $\tau_L = \mathcal{O}(\sqrt{N})$, and $\tau_{l-1} \approx \tau_l/2$ for $l < L$. Therefore, $N_l(\tau_l + 1)^2 = \mathcal{O}(N)$ and $C = \mathcal{O}(N \log N)$. For approximate forms, we simply reduce the truncation numbers as $\tau_l^\alpha \approx \alpha \tau_l$ for $\alpha \in [0, 1)$, leading to a reduced cost as

$$C \approx c_0 N_{\text{near}} + \alpha^2 \sum_{l=1}^L c_l N_l (\tau_l + 1)^2. \quad (5.2)$$

It should be noted that near-zone interactions, which are computed once at the beginning of the optimizations, are not modified. The usage of near-zone interactions is efficient since c_0 is small, while their accuracy is more critical compared to far-zone interactions.

The approximation factor α in Equation 5.2 can be used as a parameter in the optimizations in order to reduce the total optimization time. If α is chosen properly for different trials encountered in an optimization, it may decrease the optimization time significantly without decreasing the quality of the results.

In an optimization, it may be tempting to choose $\alpha = 0$, which corresponds to a version with only near-zone interactions, to obtain very rapid optimizations. However, this may lead to unreliable final results especially when the problem geometry is electrically large. In order to prevent reduction in the quality of the results when employing approximate forms of MLFMA, a penalty strategy for each approximation factor may be employed. These penalties can be applied to the solutions that are done with lower accuracy which ensures that final results of the optimization should satisfy a specified quality threshold. More detailed explanation and proposed strategies will be demonstrated and discussed for the optimization of the cage-dipole antenna.

5.3 Optimizations of the Cage-Dipole Antenna via AMLFMA

Optimization of the antenna in Figure 4.3 to maximize the transmitted power when it is matched to 50Ω at 5.80 GHz in free space is selected as a reference problem. First, in order to observe the effects of utilizing fixed approximation factors in terms of efficiency and accuracy, ten different optimizations are carried out for $\alpha = 0.0, 0.1, 0.2, 0.4$ and 0.5 , as well as with full MLFMA which actually corresponds to the case of $\alpha = 1.0$. The results are listed in Table 5.1, where matrix-vector multiplication (MVM) times, normalized MVM times, normalized optimization times, accelerations in the optimization times with respect to the full MLFMA, and the corresponding approximate errors for different values of α are presented. The approximate error is determined by taking the full MLFMA solution as reference. There is a trade-off between the accuracy of the results and the speed of the optimizations, as expected. The determined approximate errors can be used as penalty factors, i.e., the fitness value that is obtained by using α is reduced by the corresponding approximate error.

Different strategies for the use of MLFMA and its approximate forms are proposed and examined by considering both the advantages and disadvantages of the corresponding option in terms of efficiency and accuracy. In order to benefit from the approximate forms of MLFMA to accelerate optimizations without deteriorating the reliability of the final results, we employ a strategy where the

Table 5.1: Performance Summary When Fixed Approximation Factors Are Employed During Optimizations

	AMLFMA					MLFMA
	0.0	0.1	0.2	0.4	0.5	
MVM Time (seconds)	0.2039	0.4578	0.7344	1.0969	1.5788	4.530
Normalized MVM Time	0.0450	0.1011	0.1621	0.2422	0.3486	1.000
Normalized Opt. Time	0.5580	1.450	2.241	3.433	4.868	13.69
Acceleration in Opt. Time	$\times 24.5$	$\times 9.44$	$\times 6.11$	$\times 3.99$	$\times 2.81$	$\times 1.00$
Approximate Error	13.5%	8.38%	4.26%	2.35%	0.35%	0.00%

approximation factor is an optimization parameter hence becomes a part of the chromosomes of the individuals in GAs. Specifically, in addition to representing a configuration of the connections, each individual contains an information on how accurate the configuration should be analyzed. In order to reflect the cost of the approximations, the success rates of individuals are reduced by the corresponding unreliability factors which are listed in Table 5.1. Thus, individuals with accurate solutions are promoted provided that they represent successful configurations. At the same time, inaccurate solutions are also promoted if the configurations provide very good transmission coefficients.

Two dynamic strategies are proposed and examined in addition to fixed-error optimizations. Strategy-1 allows the individuals in genetic algorithm to use $\alpha = 0.0, 0.1, 0.2, 0.4, 0.5$, or full MLFMA. An approximation factor is assigned randomly to each individual in the initial population. As a part of the chromosome, the approximation factor is manipulated by genetic operations, such as crossover, mutation, and elitism. This strategy leaves the approximation factor as flexible as possible, and let the genetic algorithm select the best combinations during the optimizations. The strategy provides very accurate and high quality results at the end of the optimization with a 2.69 times speedup with respect to full MLFMA as seen in Table 5.2. On the other hand, when the performance of Strategy-1 is compared with the results obtained with fixed approximation

Table5.2: Different Strategies For the Usage of MLFMA and Its Approximate Forms on the Optimizations of the Antenna Depicted in Figure 4.3

	Normalized Opt. Time	Acceleration in Opt. Time	Approximate Error
AMLFMA(0.0)	0.5580	$\times 24.5$	13.5%
AMLFMA(0.2)	2.241	$\times 6.11$	4.26%
AMLFMA(0.4)	3.433	$\times 3.99$	2.35%
AMLFMA(0.5)	4.868	$\times 2.81$	0.35%
MLFMA	13.69	$\times 1.00$	0.00%
Strategy-1	5.086	$\times 2.69$	0.75%
Strategy-2	2.556	$\times 5.36$	1.15%

factors, it is seen that using $\alpha = 0.5$ provides more efficient and rapid optimizations. When the generated populations during the optimizations via Strategy-1 are examined, it is observed that the individuals using full MLFMA dominates the pool quickly due to their superior fitness values as their fitness values are not punished with a penalty. Hence, using MLFMA in many trials increase the total optimization time, making Strategy-1 inefficient.

Strategy-2 is very similar to Strategy-1 except that it does not allow the individuals to use full MLFMA as an option. Main purpose behind this idea is to increase the optimization speed. Strategy-2 increases the optimization speed by 5.36 fold with an approximate error of 1.15%. Comparing the results, this strategy is both faster and yield more accurate results than the strategy using a fixed $\alpha = 0.4$. Therefore, it is suggested that employing a dynamic accuracy control over the optimization procedure may provide better performance instead of using a fixed approximation factor.

The results above belong only to a specific geometry with a largest electrical size of 1.3λ . Hence, even $\alpha = 0.0$ may seem an appropriate choice due to its significant speed and a reasonable error. However, its usage in larger problems may yield very large errors in the final results. To make a more comprehensive observation, Strategy-2 is further tested in the optimization of the same antenna when it is mounted on a $4\lambda \times 4\lambda$ platform.

5.4 Optimization of the Cage-Dipole Antenna on a $4\lambda \times 4\lambda$ Platform via AMLFMA

The cage-dipole antenna when it is mounted on a large patch with an electrical size of $4\lambda \times 4\lambda$ is depicted in Figure 5.1. MLFMA uses 5 levels due to the size of the problem and the problem geometry is discretized with 15015 RWG functions to expand equivalent currents while the isolated antenna is discretized only with 455 RWG functions. Therefore, the effects of the approximate forms of MLFMA should be different in terms of accuracy and speed of the solutions. Average errors for different approximation factors are found by solving ten different problems and taking the average of their errors. These errors and the used harmonics for each approximation factor are shown in Table 5.3.

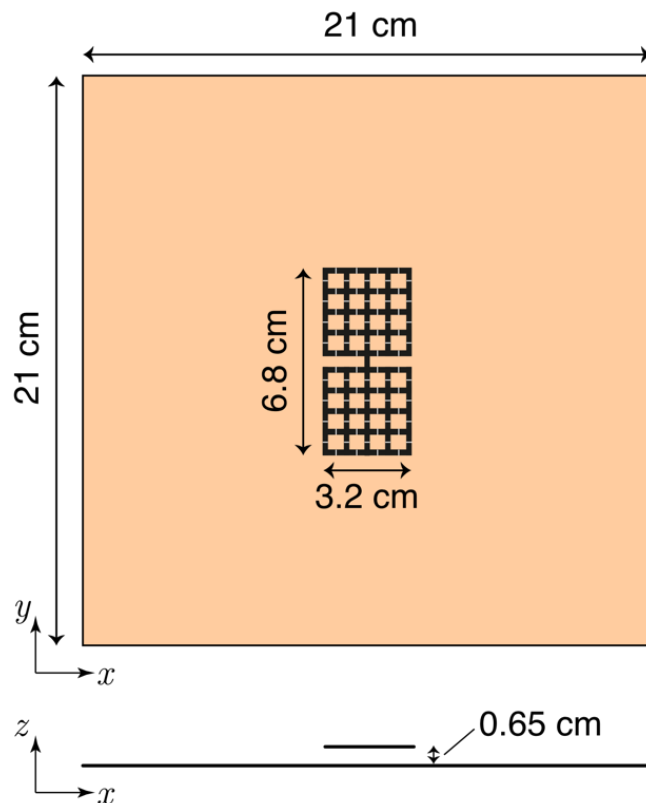


Figure 5.1: A cage-dipole antenna involving a total of 2×40 switches on $21 \text{ cm} \times 21 \text{ cm}$ patch.

Table5.3: Number of Harmonics Used for Different Values of Approximation Factor For a 5-Level MLFMA

AMLFMA	Harmonics	Average Error (Unreliability)
0.0	0,0,0	48.7%
0.1	2,1,1	44.8%
0.2	3,2,1	23.8%
0.3	5,3,2	22.3%
0.4	7,4,3	16.2%
0.5	9,5,3	9.82%
0.6	10,6,4	3.36%
0.7	12,7,5	1.14%
0.8	14,8,5	1.07%
0.9	16,10,6	0.07%
1.0	17,11,7	0.00%

Table5.4: Performance Summary of Different Approximation Factors For the Problem Depicted in Figure 5.1

	AMLFMA						MLFMA
	0.0	0.2	0.4	0.5	0.6	0.8	
MVM Time (seconds)	13.1	23.6	47.8	58.3	69.7	108	165
Normalized MVM Time	0.079	0.143	0.289	0.352	0.422	0.656	1.000
Approximate Error	48.7%	23.8%	16.2%	9.82%	3.36%	1.07%	0.00%

Strategy-2 is applied for this large geometry by allowing the individuals to use $\alpha = 0.0, 0.2, 0.4, 0.5, 0.6$ and 0.8 . MVM times in seconds, normalized MVM times, and approximate error values for these values of α are listed in Table 5.4.

The obtained results from the optimizations using AMLFMA(0.0), MLFMA, and Strategy-2 are finally listed in Table 5.5. The overall optimization with Strategy-2 takes approximately 13 hours in the MATLAB environment on a single processor. The same optimization can be done in more than two days if full MLFMA is used, without a significant improvement in the final result.

Table5.5: Results With Different Strategies For the Transmission Coefficient Optimization of the Geometry Shown in Figure 5.1

	Optimization Result	Confirmed Result	Total Time (sec)
AMLFMA(0.0)	0.9945	0.7916	8966
MLFMA	0.9977	0.9977	178225
Strategy-2	0.8957	0.9439	47371

5.5 Remarks

In this chapter, dynamic accuracy control over the optimizations using AMLFMA is presented. Some of the underlined points can be listed as follows.

- The results obtained via AMLFMA with different approximation factors are compared with the ones obtained via full MLFMA in terms of speed and accuracy.
- A penalty strategy is utilized when solutions with lower accuracy are used in optimizations in order to maintain the quality of the final results.
- Different strategies employing AMLFMA for the optimizations are discussed.

CHAPTER 6

CONCLUSION

An efficient and accurate mechanism based on heuristic algorithms and full-wave solutions via MLFMA for the optimizations of antenna excitations in array configurations and geometry optimizations of different pixel antennas are presented. Since heuristic algorithms are implemented in-house, the interactions between the full-wave solver and the optimizer modules are established efficiently instead of a black-box interaction. Moreover, the development studies on heuristic algorithms are presented with alternative methods. Excitation optimizations of the antenna arrays are tested via numerical experiments and it is shown that the proposed mechanism provides very good results even when the optimization space is extremely large. For the geometry optimizations, two different antennas are optimized efficiently by using the advantages of MLFMA. Since the setup stage of MLFMA is done once for each antenna geometry and can be used many times during the optimizations, required computational time is reduced significantly. The optimized pixel antennas are further produced via commercial printers by using silver-based toners. Challenges regarding the inkjet antenna production are briefly discussed. Produced antennas are measured, and it is observed that simulation and measurement results agree. Finally, the use of approximate forms of MLFMA to increase the speed of the optimization mechanism is discussed. It is shown that a dynamic control over the accuracy of the full-wave solutions can be utilized such that optimization times may be reduced significantly without sacrificing the quality of the final results.

The optimization environment is open to further developments since each part

of the optimization environment, i.e., electromagnetic solver and heuristic algorithms, are implemented in house. Some of the possible ways to improve the optimization mechanism in the future works can be listed as follows.

- Dynamic control over the parameters of heuristic algorithms can be utilized for more efficient optimizations.
- More advanced and accurate models can be used for the feed ports of the antennas to account for the effects of different feeding methods.
- Dynamic accuracy control using AMLFMA can be analyzed in more detail for different antenna problems involving larger unknowns, and more efficient optimization strategies employing AMLFMA can be developed.

REFERENCES

- [1] O. Ergul and L. Gurel, *The Multilevel Fast Multipole Algorithm for Solving Large-Scale Computational Electromagnetics*. IEEE-Wiley, 2014.
- [2] Y. Rahmat-Samii and E. Michielssen, *Electromagnetic optimization by genetic algorithms*. Wiley, 1999.
- [3] O. Abdul-Rahman, M. Munetomo, and K. Akama, "An improved binary-real coded genetic algorithm for real parameter optimization," in *2011 Third World Congress on Proc. Nature and Biologically Inspired Computing (NaBIC)*, Oct. 2011, pp. 149-155.
- [4] C. R. Reeves, "Using genetic algorithms with small populations," in *Proc. Fifth Int. Conf. on Genetic Algorithms*, 1993, pp. 92-99.
- [5] J. Alander, "On optimal population size of genetic algorithms," in *Proc. IEEE Int. Conf. Comput. Syst. Soft. Eng.*, May 1992 pp. 65-70.
- [6] K. D. Lu, G. Q. Zeng, J. Chen, W. W. Peng, Z.-J. Zhang, Y.-X. Dai, and Q. Wu, "Comparison of binary coded genetic algorithms with different selection strategies for continuous optimization problems," in *Chinese Automation Congress (CAC)*, Nov. 2013, pp. 364-368.
- [7] L. D. Whitley, "The genitor algorithm and selection pressure: Why rank-based allocation of reproductive trials is best.," *Proc. 3rd Int. Conf. Genetic Algorithms and Their Applications*, pp. 116-121, 1989.
- [8] H. Xie and M. Zhang, "Parent selection pressure auto-tuning for tournament selection in genetic programming," *IEEE Transactions on Evolutionary Computation*, vol. 17, pp. 1-19, Feb. 2013.
- [9] K. A. De Jong, "Analysis of the behavior of a class of genetic adaptive systems," Ph.D. dissertation, Dept. Comput. Sci. Univ. Michigan, Ann Arbor, 1975.
- [10] J. Kennedy and R. Eberhart, "Particle swarm optimization," in *Proc. IEEE International Conference on Neural Networks*, vol. 4, Nov. 1995, pp. 1942-1948.
- [11] A. Lazinica, *Particle Swarm Optimization*. In-Tech, 2009.
- [12] R. Eberhart and Y. Shi, "Particle swarm optimization: developments, applications and resources," in *Proceedings of Congress on Evolutionary Computation*, vol. 1, 2001, pp. 81-86.
- [13] J. Robinson and Y. Rahmat-Samii, "Particle swarm optimization in electromagnetics," *IEEE Transactions on Antennas and Propagation*, vol. 52, pp. 397-407, Feb. 2004.

- [14] C. A. Balanis, *Antenna theory: analysis and design*. Wiley, 2005.
- [15] E. Du Fort, “Pattern synthesis based on adaptive array theory,” *IEEE Transactions on Antennas and Propagation*, vol. 37, pp. 1011–1018, Aug. 1989.
- [16] O. Bucci, G. D’Elia, G. Mazzarella, and G. Panariello, “Antenna pattern synthesis: a new general approach,” *Proceedings of the IEEE*, vol. 82, pp. 358–371, Mar. 1994.
- [17] I. Gupta and A. Ksienski, “Effect of mutual coupling on the performance of adaptive arrays,” *IEEE Transactions on Antennas and Propagation*, vol. 31, pp. 785–791, Sep. 1983.
- [18] S. Rao, D. Wilton, and A. Glisson, “Electromagnetic scattering by surfaces of arbitrary shape,” *IEEE Transactions on Antennas and Propagation*, vol. 30, pp. 409–418, May 1982.
- [19] D. W. Zingg, M. Nemec, and T. H. Pulliam, “A comparative evaluation of genetic and gradient-based algorithms applied to aerodynamic optimization,” *European Journal of Computational Mechanics/Revue Européenne de Mécanique Numérique*, vol. 17, pp. 103–126, 2008.
- [20] J. A. Snyman, *Practical mathematical optimization : an introduction to basic optimization theory and classical and new gradient-based algorithms*. Applied Optimization Series, New York: Springer, 2005.
- [21] R. Faber, H. Arellano-Garcia, and G. Wozny, “A hybrid optimization approach to parameter estimation,” in *Proc. 17th European Symposium on Computer Aided Process Engineering*, 2007.
- [22] J. Vesterstrom and R. Thomsen, “A comparative study of differential evolution, particle swarm optimization, and evolutionary algorithms on numerical benchmark problems,” in *Proc. Congress on Evolutionary Computation*, vol.2, Jun. 2004, pp. 1980-1987.
- [23] D. S. Linden, “Automated design and optimization of wire antennas using genetic algorithms,” tech. rep., DTIC Document, 1997.
- [24] J. Robinson, S. Sinton, and Y. Rahmat-Samii, “Particle swarm, genetic algorithm, and their hybrids: optimization of a profiled corrugated horn antenna,” in *Proc. IEEE Antennas and Propagation Society International Symposium*, vol. 1, 2002, pp. 314-317.
- [25] C. A. Balanis, *Modern Antenna Handbook*. Wiley, 2008.
- [26] D. M. Pozar and S. D. Targonski, “A shared-aperture dual-band dual-polarized microstrip array,” *IEEE Transactions on Antennas and Propagation*, vol. 49, pp. 150–157, Feb. 2001.
- [27] S. Goudos, V. Moysiadou, T. Samaras, K. Siakavara, and J. Sahalos, “Application of a comprehensive learning particle swarm optimizer to unequally spaced linear array synthesis with sidelobe level suppression and null control,” *IEEE Antennas and Wireless Propagation Letters*, vol. 9, pp. 125–129, 2010.

- [28] M. Khodier and C. Christodoulou, "Linear array geometry synthesis with minimum sidelobe level and null control using particle swarm optimization," *IEEE Transactions on Antennas and Propagation*, vol. 53, pp. 2674–2679, Aug. 2005.
- [29] E. Erdil, K. Topalli, M. Unlu, O. Civi, and T. Akin, "Frequency tunable microstrip patch antenna using rf mems technology," *IEEE Transactions on Antennas and Propagation*, vol. 55, pp. 1193–1196, Apr. 2007.
- [30] D. Rodrigo and L. Jofre, "Frequency and radiation pattern reconfigurability of a multi-size pixel antenna," *IEEE Transactions on Antennas and Propagation*, vol. 60, pp. 2219–2225, May 2012.
- [31] J. Kataja, S. Jarvenpaa, J. Toivanen, R. Makinen, and P. Yla-Oijala, "Shape sensitivity analysis and gradient-based optimization of large structures using mlfma," *IEEE Transactions on Antennas and Propagation*, vol. 62, pp. 5610–5618, Nov. 2014.
- [32] O. Ozgun, S. Mutlu, M. Aksun, and L. Alatan, "Design of dual-frequency probe-fed microstrip antennas with genetic optimization algorithm," *IEEE Transactions on Antennas and Propagation*, vol. 51, pp. 1947–1954, Aug. 2003.
- [33] H. Rajagopalan, J. Kovitz, and Y. Rahmat-Samii, "Mems reconfigurable optimized e-shaped patch antenna design for cognitive radio," *IEEE Transactions on Antennas and Propagation*, vol. 62, pp. 1056–1064, Mar. 2014.
- [34] J. Martinez-Fernandez, J. Gil, and J. Zapata, "Ultrawideband optimized profile monopole antenna by means of simulated annealing algorithm and the finite element method," *IEEE Transactions on Antennas and Propagation*, vol. 55, pp. 1826–1832, Jun. 2007.
- [35] J. Araque Quijano and G. Vecchi, "Optimization of an innovative type of compact frequency-reconfigurable antenna," *IEEE Transactions on Antennas and Propagation*, vol. 57, pp. 9–18, Jan. 2009.
- [36] L. Pringle, P. Harms, S. Blalock, G. Kiesel, E. Kuster, P. Friederich, R. Prado, J. Morris, and G. Smith, "A reconfigurable aperture antenna based on switched links between electrically small metallic patches," *IEEE Transactions on Antennas and Propagation*, vol. 52, pp. 1434–1445, Jun. 2004.
- [37] C. Coleman, E. Rothwell, and J. Ross, "Investigation of simulated annealing, ant-colony optimization, and genetic algorithms for self-structuring antennas," *IEEE Transactions on Antennas and Propagation*, vol. 52, pp. 1007–1014, Apr. 2004.
- [38] S. Song and R. Murch, "An efficient approach for optimizing frequency reconfigurable pixel antennas using genetic algorithms," *IEEE Transactions on Antennas and Propagation*, vol. 62, pp. 609–620, Feb. 2014.
- [39] J. Araque Quijano and G. Vecchi, "Optimization of a compact frequency- and environment-reconfigurable antenna," *IEEE Transactions on Antennas and Propagation*, vol. 60, pp. 2682–2689, Jun. 2012.

- [40] C.-H. Wang, H.-L. Liu, and C.-T. Lin, "Dynamic optimal learning rates of a certain class of fuzzy neural networks and its applications with genetic algorithm," *IEEE Transactions on Systems, Man, and Cybernetics, Part B: Cybernetics*, vol. 31, pp. 467–475, Jun. 2001.
- [41] A. Rida, L. Yang, R. Vyas, and M. Tentzeris, "Conductive inkjet-printed antennas on flexible low-cost paper-based substrates for rfid and wsn applications," *IEEE Antennas and Propagation Magazine*, vol. 51, pp. 13–23, Jun. 2009.
- [42] N. Rajasekhar and K. Anusudha, "Dual band microstrip antenna with dumbbell slot for wimax/wlan/satellite communications," in *Proc. International Conference on Microwave and Photonics (ICMAP)*, Dec. 2013, pp. 1-6.
- [43] W. C. Chew, E. Michielssen, J. Song, and J. Jin, *Fast and efficient algorithms in computational electromagnetics*. Artech House, 2001.